UNIVERSIDADE DO VALE DO RIO DOS SINOS - UNISINOS
UNIDADE ACADÊMICA DE PESQUISA E PÓS-GRADUAÇÃO
PROGRAMA DE PÓS-GRADUAÇÃO EM GEOLOGIA
NÍVEL MESTRADO

ALISSON KLAYTON MARTINS

Conexões entre a Circulação de Revolvimento do Atlântico e padrões de precipitação no nordeste da América do Sul durante o último deglacial

São Leopoldo
2021

Alisson Klayton Martins

Conexões entre padrões de precipitação no nordeste da América do Sul e a produtividade primária no oeste do Oceano Atlântico Sul durante o último deglacial

Dissertação apresentado como requisito parcial para obtenção do título de Mestre em Geologia, pelo Programa de Pós-Graduação em Geologia da Universidade do Vale do Rio dos Sinos - UNISINOS

Orientador: Prof. Dr. Karlos G. D. Kochhann

São Leopoldo

2021

RESUMO

É amplamente conhecido que as temperaturas globais e os níveis do mar estão subindo, os padrões de chuva estão mudando e os eventos climáticos extremos estão se tornando mais intensos e destrutivos. Neste sentido, a Geologia é de suma importância para entendermos como o clima se modificou no passado e auxiliar em predições de mudanças climáticas atuais e futuras. Nesta dissertação discutimos como uma mudança na Circulação Meridional de Revolvimento do Atlântico (AMOC) pode acarretar anomalias climáticas e de produtividade primária para o Oceano Atlântico Sul. A possibilidade de um colapso (ou enfraquecimento acentuado) na AMOC dentro de alguns séculos aumentou o interesse da comunidade científica nas respostas de diferentes compartimentos do sistema terrestre a colapsos anteriores de AMOC (ou enfraquecimento acentuado). Os exemplos mais recentes desses períodos são Heinrich Stadial 1 (HS1,18-15 ka BP; AMOC quase colapsada) e o Younger Dryas (YD, 12,9-11,7 ka BP; AMOC marcadamente enfraquecido). Aqui, apresentamos razões elementares, biomarcadores orgânicos, reconstruções da temperatura da superfície do mar e dados de assembleias de foraminíferos planctônicos de um testemunho de sedimento marinho recuperado do Oceano Atlântico Sul tropical ocidental que se estende pelos últimos ca. 20 ka. O testemunho registra as respostas do hidroclima da América do Sul tropical e mudanças de produtividade do Atlântico Sul tropical, durante as flutuações de intensidade de AMOC associadas com HS1 e o YD. Nossos dados mostram que tanto o HS1 quanto o YD foram caracterizados por um clima mais úmido sobre o nordeste da América do Sul tropical e, consequentemente, houve um aumento do aporte sedimentar continental. No entanto, o escoamento de sedimentos continental foi provavelmente mais intenso durante o HS1, quando o fornecimento de nutrientes

aumentou a produtividade primária no oceano Atlântico Sul tropical ocidental. Juntamente com dados publicados anteriormente, sugerimos que diminuições marcantes na intensidade de AMOC durante HS1 e o YD aprisionaram o calor na camada superficial do oeste do Oceano Atlântico Sul, facilitando a transferência de umidade e aumentando a precipitação sobre o nordeste da América do Sul.

Palavras chaves: Mudanças climáticas, Paleoclimatologia, Precipitação, América do Sul, *Heinrich Stadial*, *Younger Dryas*

ABSTRACT

It is a known-well fact that global temperatures and sea levels are rising, rainfall patterns are changing, and extreme weather events are becoming more intense and destructive. In this sense, geology plays a crucial role to understand how climate has changed in the past and assist in predictions of current and future climate shifts. In this work we discuss how a change in the Atlantic Meridional Overturning Circulation (AMOC) can cause climatic anomalies over northeastern South America. The possibility of a collapse (or sharp weakening) of the AMOC within a few centuries has increased the scientific community's interest in responses from different compartments of the Earth system to previous collapses of AMOC (or sharp weakening). The most recent examples of these periods are Heinrich Stadial 1 (HS1,18-15 ka BP; AMOC almost collapsed) and the Younger Dryas (YD, 12.9-11.7 ka BP; AMOC markedly weakened). Here, we present elemental ratios, organic biomarkers, reconstructions of sea surface temperature and data from planktonic foraminiferal assemblages of a marine sediment core recovered from the western tropical South Atlantic Ocean that extends through the last ca. 20 kyr. The core records hydroclimate responses of tropical South America and productivity changes in the western tropical South Atlantic during AMOC intensity fluctuations associated with HS1 and the YD. Our data show that both HS1 and the YD were characterized by wetter climates over the northeastern South America and, consequently, there was an increase in continental runoff. However, continental runoff was probably more intense during HS1, when nutrient supply increased primary productivity in the western tropical South Atlantic Ocean. Together with previously published data, we suggest that marked decreases in AMOC intensity during HS1 and the YD trapped

heat in the surface layer of the western South Atlantic Ocean, facilitating humidity transfer and increasing precipitation over northeastern South America.

Keywords: Climate change, Paleoclimatology, Precipitation, South America, Heinrich Stadium, Younger Dryas

Apresentação

Nesta dissertação intitulada de “Conexões entre padrões de precipitação no nordeste da América do Sul e a produtividade primária no oeste do Oceano Atlântico Sul durante o último deglacial”, serão apresentados estudos de dois anos de trabalho. Os dados obtidos trata-se de um estudo multi proxie, onde foi feito ciência em colaboração com vários pesquisados das áreas de Paleoclimatologia e Paleoceanografia. Fica então meu agradecimento em especial aos meus colaboradores: Tamires Zardin por ter realizado a triagem do dos foraminíferos planctônicos; Cristiano Chiessi, Marília Campos Stefano Crivellari, André Bahr e Henning Kuhnert, pelos dados da técnica de Mg/Ca que possibilitou um ótimo resultado para o estudo; Lorenz Schwark e Thosthen Bauersachs por terem me recebido em Kiel na Alemanha e por terem auxiliado com biomarcadores orgânicos moleculares; Guilherme Krahl, Lais Vieira e Gerson Fauth pela ajuda com as técnicas químicas realizadas no testemunho. E ao meu orientador Karlos Kochhann que de forma leve e tranquila me passou um conhecimento científico muito rico e me fez amar ainda mais a ciência.

SUMÁRIO

1.INTRODUÇÃO

Esta dissertação aborda diversos métodos para reconstruções paleoclimáticas, resultando no manuscrito intitulado de "*Links between precipitation patterns over eastern tropical South America and primary productivity in the western tropical South Atlantic Ocean during the last 20 kyr".* Durante o decorrer do mestrado foram utilizadas diversas metodologias de química analítica (*proxies* geoquímicos) em um testemunho sedimentar localizado na Bacia de Sergipe-Alagoas, próximo à foz do Rio São Francisco, cujos sedimentos abrangem o Quaternário tardio. O estudo visa testar a hipótese de que eventos paleoceanográficos e paleoclimáticos impactaram no aporte de sedimentos e água setor oeste do Oceano Atlântico Sul tropical nos últimos 20 ka. O manuscrito gerado foi submetido ao periódico *Palaeogeography, Palaeoclimatology, Palaeoecology*.

Em relação a temática e problema discutidos no artigo científico, já é sabido que o transporte de calor oceânico cruzando a região equatorial em direção ao hemisfério norte é de cerca de 0,5 PW por ano, sendo ocasionado, principalmente, pela circulação de revolvimento meridional do Atlântico (*Atlantic Meridional Overturning Circulation* - AMOC). Esse fenômeno resulta em águas superficiais relativamente quentes no Oceano Atlântico Norte, tornando o hemisfério norte mais quente do que o hemisfério sul (Mohtadi et al., 2016). Em resposta, há um transporte de energia em direção ao hemisfério sul por meio da circulação atmosférica de Hadley, posicionando o ramo ascendente da circulação de Hadley e a posição média da Zona de Convergência Intertropical (ITCZ) (ver Fig. 1) ao norte do Equador (Schneider et al., 2014). Segundo Mohtadi et al. (2016), qualquer mecanismo físico que induz o aquecimento ou

resfriamento anômalo de um hemisfério em relação ao outro deslocará a posição média do ITCZ em direção ao hemisfério em aquecimento, o que afetará os sistemas de monções tropicais.

No que se refere a variações de intensidade da AMOC e deslocamentos da ITCZ ao longo do tempo, o maior corpo de dados existente refere-se ao último estágio Heinrich (HS1, cerca de 18-15 ka antes do presente). Durante o evento HS1, a AMOC estava quase colapsada e as temperaturas da superfície do Atlântico Norte eram mínimas (McManus et al., 2004). Uma compilação global dos registros paleo-hidrológicos disponíveis para o evento HS1 sugere que houve um deslocamento do ITCZ para o sul associado com a mudança de assimetria térmica inter-hemisférica (Mohtadi et al., 2016). Portanto, é esperado que em intervalos de tempo em que a AMOC esteve enfraquecida ou quase colapsada, anomalias de precipitação e temperatura (aquecimento) ocorreram em diversas regiões do hemisfério sul (Campos et al., 2019; Crivellari et al., 2019).

Neste sentido foi escolhido um testemunho de sondagem marinho estratégico para definir eventos que registram anomalias climáticas e oceanográficas, localizado próximo à foz do Rio São Francisco. No leste do Brasil, a influência da Zona de Convergência do Atlântico Sul se expande sobre a área proximal da bacia de drenagem do Rio São Francisco (Stríkis et al., 2015). Após seguir seu curso rumo à região nordeste, o Rio São Francisco desagua em uma área do Oceano Atlântico Sul influenciada pela Corrente Norte do Brasil (superficial), Contracorrente Norte do Brasil (em profundidades intermediárias) e Água Profunda do Atlântico Norte (a grandes profundidades) (Stramma e England, 1999). Com base nessa configuração climática e

oceanográfica, nossa proposta de pesquisa assume que sedimentos quaternários depositados em posição distal à foz do Rio São Francisco têm o potencial de registrar mudanças na atividade das monções por meio de registros geoquímicos, isotópicos e faunísticos.

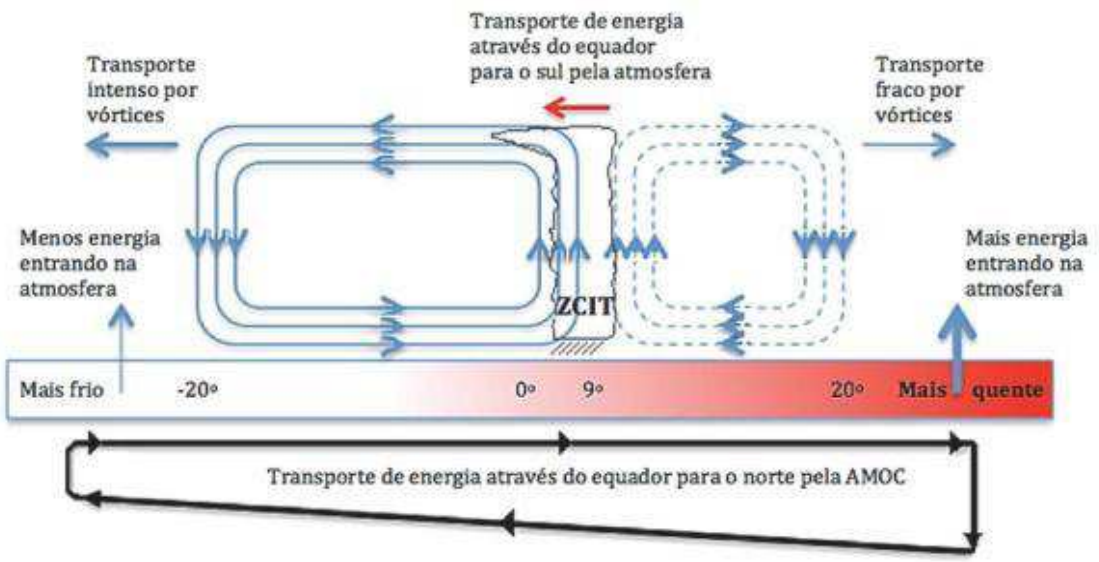

Figura 1: Esquema ilustrativo da conexão entre AMOC e a célula de Hadley com média da ITCZ em 9º ao norte do equador. Por ser mais aquecido, o Hemisfério Norte libera mais radiação de ondas longas para a atmosfera do que o Hemisfério Sul, devido ao transporte de energia na direção do Hemisfério Norte promovido pela AMOC. Paralelamente, a circulação de Hadley transporta umidade para o Hemisfério Norte em superfície, e energia para o Hemisfério Sul. Uma parte da energia também é transportada por vórtices atmosféricos que são gerados nos flancos subtropicais da célula de Hadley. Baseado em (Frierson e Hwang, 2012) e retirado de (Aimola e Moura, 2016).

2. ATLANTIC MERIDIONAL OVERTURNING CIRCULATION (AMOC)

A AMOC é considerada um padrão de circulação de grande escala que transporta águas superficiais e quentes em direção às altas latitudes do Atlântico Norte, e retorna trazendo águas profundas e frias para o Atlântico Sul (Bryden et al., 2005; Cunningham et al., 2007). É amplamente discutido que a AMOC pode ser composta por quatro ramos principais: (1) ressurgências, - que transportam águas de fundo para a superfície – (2) correntes superficiais, que transportam águas de baixa densidade em direção às altas latitudes; (3) regiões de formação de águas profundas (FAP) – águas se tornam mais densas e afundam – (4) correntes profundas, que transportam águas de alta densidade encerrando esse revolvimento desenvolvido pela AMOC (Kuhlbrodt et al., 2007)

Neste sentido, é possível compreender que a AMOC possui uma grande importância no que tange ao clima global. Esse mecanismo exerce forte controle na estratificação e distribuição de massas de água, na quantidade de calor que é transportada pelo oceano e no ciclo de estocagem de espécies químicas (CO_2) no mar profundo (Kuhlbrodt et al., 2007).

No passado a AMOC já passou por oscilações. Um bom exemplo ocorreu no último período glacial e na posterior deglaciação (McManus et al., 2004). Seu enfraquecimento mostrou-se capaz de afetar o clima de forma significativa, provocando inúmeras anomalias climáticas, sendo algumas delas: (1) resfriamento das altas latitudes do Atlântico Norte (Bard et al., 2000), (2) aquecimento da superfície do Oceano Atlântico Sul (Chiessi et al., 2015), (3) aumento do CO_2 atmosférico (Kearey and Brooks, n.d.) (4) mudanças na

posição da Zona de Convergência Intertropical (ZCIT - Campos et al., 2020; Venancio et al., 2020), (5) alterações nos ecossistemas marinhos em todo o Oceano Atlântico (Portilho-Ramos et al., 2017; Schmittner, 2005) e (5) e modificações no nível do mar no Atlântico Norte (Levermann et al., 2005).

3. SISTEMA DE MONÇÃO

Um Sistema de Monção é caracterizado pela diferença de temperatura existente entre um certo continente e o oceano adjacente que produz uma reversão sazonal dos ventos em baixos níveis. Então, o continente responde á insolação de forma rápida, aquecendo e resfriando em um período menor que o Oceano o faz. Essa troca ocorre uma vez que a capacidade térmica do continente é menor que a do oceano (Mohtadi et al., 2016).

No verão, há um rápido aquecimento do continente e um aquecimento mais lento do oceano, o que cria um gradiente de temperatura e pressão entre eles. No continente, esse aquecimento provoca a expansão e ascensão do ar superficial. Então, essa movimentação de ar origina uma zona de baixa pressão sobre o continente, que acaba atraindo ar do oceano (zona de alta pressão). Esse ar atraído também é aquecido sofrendo expansão e ascensão. Esse movimento de ar oceano-continente carrega a umidade, contribuindo para as chuvas de monções (Mohtadi et al., 2016).

No entanto, na América do sul não ocorre a completa reversão sazonal dos ventos de baixos níveis, que se trata de um mecanismo típicos das Monções Asiáticas. Ao longo do ano ocorre um deslocamento dos alísios no sentido oceano-continente. Esse fenômeno tem sido denominado de "*moonson-like*" ou Sistema de Monção da América do Sul (SMAS). Esse

sistema também é marcado por mostrar variações sazonais como fortalecimento no verão austral e enfraquecimento no inverso austral (Garreaud et al., 2009). Para a área estudada nessa dissertação (nordeste da América do Sul), dados de modelos climáticos e oceanográficos não mostram um forte desenvolvimento do SMAS (Campos et al., 2019). Essas informações serão melhores discutidas também por proxies abordados no manuscrito.

4. VARIAÇÕES CLIMÁTICAS DA AMOC DURANTE O *HEINRICH STADIAL* E O *YOUGER DRYAS*

A variabilidade climática de escala milenar afeta diversos compartimentos do sitema Terra (Barker et al., 2009). Acredita-se que exista um efeito “gangorra” (*bipolar seesaw)* entre os hemisférios Sul e Norte, onde ocorre um resfriamento no Hemisfério Norte concomitante a um aquecimento no Hemisfério Sul, e vice-versa. As variações na intensidade da AMOC acabam por afetar a distribuição de calor entre os oceanos Atlântico Sul e Norte, sendo assim o principal agente desse efeito “gangorra” (Barker et al., 2009; Chiessi et al., 2015).

Quando ocorre um enfraquecimento da AMOC devido à uma grande quantidade de água doce adicionada ao Oceano Atlântico Norte (acentuada por descarga e degelo icebergs), há um decréscimo do transporte de calor em direção ao Atlântico Norte. A resultante desse processo é um acúmulo de calor no Hemisfério Sul, tornando a temperatura da superfície oceânica do Atlântico Sul mais quente que a do Atlântico Norte (Barker et al., 2009).

Registros da razão $^{231}Pa/^{230}Th$ obtida a partir de um testemunho sedimentar da porção noroeste subtropical do Atlântico, foram utilizados como um proxy para a intensidade da AMOC (Böhm et al., 2014): quanto maior a razão, menor é a intensidade da AMOC, indicando fluxo mais lento e mais raso da Água profunda do Atlântico Norte (APAN). Esses autores mostraram que, durante os últimos 140 mil anos, a AMOC passou por diferentes modos de funcionamento sendo eles: (1) *warm mode* – onde atuam a APAN e a Água Antártica de Fundo (AAF); (2) *cold mode* – onde atuam a APAN e a AAF, porém a APAN encontra-se enfraquecida e mais rasa; e (3) *off mode,* também chamado de *Heinrich mode* onde a APAN é desligada atuando somente a AAF.

Dados de um testemunho sedimentar do Atlântico Norte estudado por McManus et al. (2004) também mostram que durante o Último Máximo Glacial (~23 e 19 ka) a AMOC esteve 30-40% mais fraca, quando comparada ao Holoceno. Além disso, McManus et al. (2004) indicam que a intensidade da AMOC nos últimos 20 ka não foi constante. A AMOC estava colapsada durante o *Heinrich Stadial 1* (HS1) e enfraquecida durante o *Younger Dryas* (YD).

Esses estudos citados acima, mostram que os eventos HS1 e YD são de grande importância para entender o funcionamento da AMOC. Apesar de existirem inúmeros trabalhos sobre o tema para o Atlântico Norte, o Oceano Atlântico Sul ainda carece de estudos. O Manuscrito a seguir visa contribuir para o entendimento dos impactos de mudanças de intensidade da AMOC na região nordeste da América do Sul.

5. REFERÊNCIAS

Aimola, L., Moura, M., 2016. A Influência da Circulação de Revolvimento Meridional do Atlântico na Definição da Posição Média da ZCIT ao Norte do Equador. Uma Revisão. Rev. Bras. Meteorol. 31, 555–563. https://doi.org/10.1590/0102-7786312314b20150059

Bard, E., Rostek, F., Turon JL, Gendreau S, 2000. Hydrological impact of heinrich events in the subtropical northeast atlantic. Science 289, 1321–1324. https://doi.org/10.1126/SCIENCE.289.5483.1321

Barker, S., Diz, P., Vautravers, M.J., Pike, J., Knorr, G., Hall, I.R., Broecker, W.S., 2009. Interhemispheric Atlantic seesaw response during the last deglaciation. Nature 457, 1097–1102. https://doi.org/10.1038/nature07770

Böhm, E., Lippold, J., Gutjahr, M., Frank, M., Blaser, P., Antz, B., Fohlmeister, J., Frank, N., Andersen, M.B., Deininger, M., 2014. Strong and deep Atlantic meridional overturning circulation during the last glacial cycle. Nat. 2014 5177532 517, 73–76. https://doi.org/10.1038/nature14059

Bryden, H.L., Longworth, H.R., Cunningham, S.A., 2005. Slowing of the Atlantic meridional overturning circulation at 25° N. Nature 438, 655–657. https://doi.org/10.1038/nature04385

Campos, M.C., Chiessi, C.M., Prange, M., Mulitza, S., Kuhnert, H., Paul, A., Venancio, I.M., Albuquerque, A.L.S., Cruz, F.W., Bahr, A., 2019. A new mechanism for millennial scale positive precipitation anomalies over tropical South America. Quat. Sci. Rev. 225. https://doi.org/10.1016/j.quascirev.2019.105990

Campos, M.C., Chiessi, C.M., Venancio, I.M., Pinho, T.M.L., Crivellari, S., Kuhnert, H., Schmiedl, G., Díaz, R.A., Albuquerque, A.L.S., Portilho-Ramos, R.C., Bahr, A., Mulitza, S., 2020. Constraining Millennial-Scale Changes in Northern Component Water Ventilation in the Western Tropical South Atlantic, Paleoceanography and Paleoclimatology. https://doi.org/10.1029/2020PA003876

Chiessi, C.M., Mulitza, S., Mollenhauer, G., Silva, J.B., Groeneveld, J., Prange, M., 2015. Thermal evolution of the western South Atlantic and the adjacent continent during Termination 1. Clim. Past 11, 915–929. https://doi.org/10.5194/CP-11-915-2015

198 Crivellari, S., Chiessi, C.M., Kuhnert, H., Häggi, C., Mollenhauer, G., Hefter, J.,
199 Portilho-Ramos, R., Schefuß, E., Mulitza, S., 2019. Thermal response of
200 the western tropical Atlantic to slowdown of the Atlantic Meridional
201 Overturning Circulation. Earth Planet. Sci. Lett. 519, 120–129.
202 https://doi.org/10.1016/j.epsl.2019.05.006
203 Cunningham, S.A., Kanzow, T., Rayner, D., Baringer, M.O., Johns, W.E.,
204 Marotzke, J., Longworth, H.R., Grant, E.M., Hirschi, J.J.-M., Beal, L.M.,
205 Meinen, C.S., Bryden, H.L., 2007. Temporal Variability of the Atlantic
206 Meridional Overturning Circulation at 26.5°N. Science (80-.). 317, 935–
207 938. https://doi.org/10.1126/SCIENCE.1141304
208 Frierson, D.M.W., Hwang, Y.-T., 2012. Extratropical Influence on ITCZ Shifts in
209 Slab Ocean Simulations of Global Warming. J. Clim. 25, 720–733.
210 https://doi.org/10.1175/JCLI-D-11-00116.1
211 Garreaud, R.D., Vuille, M., Compagnucci, R., Marengo, J., 2009. Present-day
212 South American climate. Palaeogeogr. Palaeoclimatol. Palaeoecol. 281,
213 180–195. https://doi.org/10.1016/J.PALAEO.2007.10.032
214 Kearey, P., Brooks, I.M., n.d. Introdução À Geofísica De Exploração.
215 Kuhlbrodt, T., Griesel, A., Montoya, M., Levermann, A., Hofmann, M.,
216 Rahmstorf, S., 2007. On the driving processes of the Atlantic meridional
217 overturning circulation. Rev. Geophys. 45.
218 https://doi.org/10.1029/2004RG000166
219 Levermann, A., Griesel, A., Hofmann, M., Montoya, M., Rahmstorf, S., 2005.
220 Dynamic sea level changes following changes in the thermohaline
221 circulation. Clim. Dyn. 2005 244 24, 347–354.
222 https://doi.org/10.1007/S00382-004-0505-Y
223 McManus, J.F., Francois, R., Gherardi, J.-M., Keigwin, L.D., Brown-Leger, S.,
224 2004. Collapse and rapid resumption of Atlantic meridional circulation
225 linked to deglacial climate changes. Nat. 2004 4286985 428, 834–837.
226 https://doi.org/10.1038/nature02494
227 Mohtadi, M., Prange, M., Steinke, S., 2016. Palaeoclimatic insights into forcing
228 and response of monsoon rainfall. Nature 533, 191–199.
229 https://doi.org/10.1038/nature17450
230 Portilho-Ramos, R.C., Chiessi, C.M., Zhang, Y., Mulitza, S., Kucera, M., Siccha,

M., Prange, M., Paul, A., 2017. Coupling of equatorial Atlantic surface stratification to glacial shifts in the tropical rainbelt. Sci. Rep. 7, 1–8. https://doi.org/10.1038/s41598-017-01629-z

Schmittner. A, 2005. Decline of the marine ecosystem caused by a reduction in the Atlantic overturning circulation. Nature 434, 628–633. https://doi.org/10.1038/NATURE03476

Schneider, T., Bischoff, T., Haug, G.H., 2014. Migrations and dynamics of the intertropical convergence zone. Nat. 2014 5137516 513, 45–53. https://doi.org/10.1038/nature13636

Stramma, L., England, M., 1999. On the water masses and mean circulation of the South Atlantic Ocean. J. Geophys. Res. Ocean. 104. https://doi.org/10.1029/1999jc900139

Stríkis, N.M., Chiessi, C.M., Cruz, F.W., Vuille, M., Cheng, H., De Souza Barreto, E.A., Mollenhauer, G., Kasten, S., Karmann, I., Edwards, R.L., Bernal, J.P., Sales, H.D.R., 2015. Timing and structure of Mega-SACZ events during Heinrich Stadial 1. Geophys. Res. Lett. 42, 5477–5484. https://doi.org/10.1002/2015GL064048

Venancio, I.M., Shimizu, M.H., Santos, T.P., Lessa, D.O., Portilho-Ramos, R.C., Chiessi, C.M., Crivellari, S., Mulitza, S., Kuhnert, H., Tiedemann, R., Vahlenkamp, M., Bickert, T., Sampaio, G., Albuquerque, A.L.S., Veiga, S., Nobre, P., Nobre, C., 2020. Changes in surface hydrography at the western tropical Atlantic during the Younger Dryas. Glob. Planet. Change 184, 103047. https://doi.org/10.1016/j.gloplacha.2019.103047

6. MANUSCRITO

Links between precipitation patterns over eastern tropical South America and primary productivity in the western tropical South Atlantic Ocean during the last deglacial

Alisson K. Martins[1]*, Karlos G. D. Kochhann[1,2], Cristiano M. Chiessi[3], Thorsten Bauersachs[4], Tamires N. Zardin[1,2], Marília C. Campos[3,5], Guilherme Krahl[1,2], Laís V. de Souza[6], Stefano Crivellari[3], André Bahr[7], Henning Kuhnert[8], Lorenz Schwark[4], Gerson Fauth[1,2]

[1]Geology Graduate Program, UNISINOS University, São Leopoldo 93022-750, Brazil

[2]Technological Institute of Micropaleontology, itt Fossil, UNISINOS University, São Leopoldo 93022-750, Brazil

[3]School of Arts, Sciences and Humanities, University of São Paulo, São Paulo 03828-000, Brazil

[4]Department of Geosciences, Christian-Albrechts-University, Kiel D-24118, Germany

[5]Institute of Geosciences, University of São Paulo, São Paulo 05508-080, Brazil

[6]VizGEO Lab, UNISINOS University, São Leopoldo 93022-750, Brazil

[7]Institute of Earth Sciences, Heidelberg University, Heidelberg D-69120, Germany

[8]MARUM—Center for Marine Environmental Sciences, University of Bremen, Bremen D-28359, Germany

*Corresponding author: Alisson K Martins (alissonkm@edu.unisinos.br)

ABSTRACT

The little considered possibility of a collapse (or marked weakening) of the Atlantic meridional overturning circulation (AMOC) within a few centuries boosted the interest of the scientific community on the responses of different compartments of the climate system to past AMOC collapses (or marked weakening). The most recent examples of such periods are Heinrich Stadial 1 (HS1,18-15 ka BP; near-collapsed AMOC) and the Younger Dryas (YD, 12.9-11.7 ka BP; markedly weakened AMOC). Here, we present elemental ratios, spectral reflectance data, organic biomarkers, sea surface temperatures reconstructions and planktonic foraminiferal assemblage data from two marine sediment core recovered from the western tropical South Atlantic Ocean that spans the last ~20 kyr. The recovered sediments record the responses of eastern tropical South American hydroclimate, western tropical South Atlantic productivity and sea surface temperatures to changes in AMOC intensity associated with HS1 and the YD. Our data show that both HS1 and the YD were characterized by a wetter climate over eastern tropical South America and increased continental runoff. High sea surface temperatures during HS1 and the

YD are in line with a marked AMOC decrease that lead to heat accumulation in the surface layer of the western South Atlantic Ocean, and facilitated moisture transfer, which increased precipitation over eastern tropical South America. Our data for the first time demonstrate that intense runoff during HS1, and hence nutrient transfer to the ocean, lead to distinctly elevated primary productivity in the otherwise oligotrophic western tropical South Atlantic Ocean. Our study thus demonstrates an intimate coupling of marine-terrestrial processes in the eastern South American realm during periods of strong climate instability.

Keywords: Quaternary; Paleoclimatology; Precipitation; Paleoproductivity; Heinrich Stadial; Younger Dryas.

6.1. INTRODUCTION

Geochemical proxies indicate that weakening of the Atlantic meridional overturning circulation (AMOC) occurred during Heinrich Stadial 1 (HS1) 18-15 thousand years before present - ka BP) (Heinrich, 1988) and the Younger Dryas (YD) 12.9-11.7 ka BP (Broecker, 1994). Although several mechanisms have been proposed to explain the HS1 and the YD deglacial coolings/oscillations (e.g., Firestone et al., 2007; Renssen et al., 2015; Sun et al., 2020; Velay-Vitow and Richard Peltier, 2020a,b) the fact that AMOC intensity was marked reduced during these events significantly affected interhemispheric heat transfer in the Atlantic Ocean (Bard et al., 2000; Barker et al., 2009; Chiessi et al., 2015). In fact, AMOC nearly collapsed during HS1 due to freshwater discharge in the high latitudes of the North Atlantic (Bond et al., 1992), and significantly weakened during the YD (McManus et al., 2004). These changes in AMOC intensity and, therefore, in the cross-equatorial heat transfer, also affected

339 South American hydroclimate (Arz et al., 1998; Campos et al., 2019; Kageyama
340 et al., 2013). Precipitation anomalies during HS1 and the YD across large parts
341 of tropical South America consequently affected the intensity of continental
342 runoff into the western tropical South Atlantic Ocean.

343 It is, however, still unclear to what extend input of nutrients supply from
344 continental runoff may have affected marine productivity in the, otherwise,
345 oligotrophic western tropical South Atlantic Ocean. For instance, riverine
346 nutrients supply likely played a significant role in boosting primary productivity in
347 the eastern tropical South Atlantic Ocean, off the Zaire Fan during the last 200
348 kyr (Holtvoeth et al., 2003; Schneider et al., 1997). During HS1, a nearly
349 collapsed AMOC (McManus et al., 2004) and a marked southward migration of
350 the Intertropical Convergence Zone (ITCZ; Mulitza et al., 2017) occurred
351 simultaneously with changes in the latitudinal position of the South Atlantic
352 Subtropical Gyre (SASG) (Pinho et al., 2021). This reorganization of South
353 Atlantic circulation likely affected primary productivity. In fact, a shallower mixed
354 layer coupled with increased surface productivity occurred during HS2, HS1 and
355 the YD in the equatorial Atlantic Ocean, an area directly affected by ITCZ shifts
356 (Portilho-Ramos et al., 2017). In the western tropical South Atlantic, however,
357 we hypothesize that increases in surface productivity could have occurred
358 during AMOC slowdown events due to: (i) increased discharge of nutrients by
359 drainage systems; and/or (ii) enhanced wind-driven upwelling intensity due to
360 reorganizations of atmospheric circulation.

361 Here we investigate climatic, hydrographic and productivity changes
362 recorded in two marine sediment cores collected near the mouth of the São
363 Francisco River, in the western tropical South Atlantic. We combined

364 geochemical and physical properties records with planktonic foraminiferal
365 assemblage data to: (i) constrain hydroclimate conditions (and continental
366 runoff) over eastern tropical South America during the last 20 kyr, associated
367 with a nearly collapsed (HS1) and a weakened (YD) AMOC; and (ii) assess
368 possible causes for the associated paleoproductivity change in the western
369 tropical South Atlantic Ocean.
370

371 **6.2. MATERIAL AND METHODS**

372 **6.2.1 Core location and sampling strategy**

373 We studied marine sediment core SEAL-20230070 (11°8S and 36°48W,
374 1300 m water depth), collected from the western tropical South Atlantic (Fig. 1).
375 The core was retrieved from the Sergipe-Alagoas Basin, on the Brazilian
376 continental margin, about 32 km from the mouth of the São Francisco River
377 (Fig. 1). The 275 cm-long sediment core consists of silty to sandy clays. In order
378 to investigate general trends and abrupt climatic events of the last 20 kyr, we
379 investigated the uppermost 190 cm of core SEAL-20230070. Sampling was
380 conducted at 2.5 cm resolution.
381 In addition, we established a sea surface temperature (SST) record
382 based on Mg/Ca ratios of the planktonic foraminiferal species *Globigerinoides*
383 *ruber pink* (ranging from 250-350 μm) from the nearby core M125-95-3 (Fig. 1).
384 The core was collected at a water depth of 1897 m (10°94S, 36°20W).
385 Sampling was conducted at 6 cm resolution in the uppermost 236 cm of the
386 clay-rich sedimentary succession. The age model for core M125-95-3 was
387 previously published in Campos et al. (2019).

388 **6.2.2 Sediment elemental ratios and spectral reflectance**

389 We measured major and trace elements in sediment samples from core
390 SEAL-20230070 with a PanAlytical Epsilon 1 X-ray fluorescence (XRF)
391 spectrometer at the Technological Institute of Micropaleontology (itt Fossil)
392 UNISINOS University, Brazil. Measurements were performed on ~10 g of dry,
393 ground and homogenized sediment samples placed in containers and covered
394 with a 3.6 µm polyester film. Results are reported as raw counts per second
395 (cps) intensities and elemental ratios are interpreted on a logarithmic basis.
396 Measurements were conducted at 10 kV (for Al, Mg, and Si), 12 kV (for Ca, K,
397 Ti, and V), 20 kV (for Co, Cr, Fe, and Mn) and 50 kV (for Ba and Rb).

398 The log(Ti/Ca) and log(Fe/Ca) ratios in marine sediments are indicative
399 of terrigenous input versus carbonate production. Fe and Ti are mostly
400 associated with terrigenous sediments, whereas Ca is primarily delivered to the
401 ocean floor as calcareous biogenic remains (e.g. Calvert and Pedersen, 2007;
402 Govin et al., 2012). The log(Fe/K) elemental ratio is interpreted as a tracer for
403 continental chemical weathering conditions and thus hydroclimate. Fe is mostly
404 delivered to ocean basins as intensely weathered particles formed under
405 relatively wet climates, while K is only present in weakly weathered particles
406 typical formed in relatively dry climates (Govin et al., 2012; Yarincik et al.,
407 2000).

408 We measured spectral reflectance at core SEAL-20230070 with a
409 Spectral Evolution (SR-35000) spectroradiometer on ~10 g aliquots of ground
410 and dry sediments. We identified 1024 spectral bands, ranging between 0.35
411 µm and 2.5 µm. Measurements were repeated three times for each sample, and
412 the average value of the three replicates was used to reduce noise of the time

series. Total reflectance (brightness – L*) was calculated following Balsam et al., (1999) and we interpret changes in L* as indicative of varying proportions between terrigenous clays (darker tones) and carbonate particles (lighter tones).

6.2.3 Planktonic foraminiferal assemblages

About 10 g of each sediment sample of core SEAL-20230070 were washed over 63 and 125 µm sieves and dried in an oven at ~40 °C for about 24 hours. Planktonic foraminiferal picking and census counts were performed on the >125 µm size fraction. We quantified absolute and relative foraminiferal abundances from residue splits containing between 300 and 600 specimens per sample. Taxonomic identifications were based on Hemleben et al. (1989) and the planktonic foraminiferal Mikrotax database (https://www.mikrotax.org/pforams/index.html).

We focused on the total abundances of planktonic foraminifera per gram of sediment, and the interpretation of relative abundances of *Globigerina bulloides*, *Trilobatus trilobus*, *T. sacullifer*, and *Globigerinoides ruber*. We also estimated changes in surface primary productivity using the index $R_{HP/Planktonic}$ (Campos et al., 2020; Portilho-Ramos et al., 2017) which is calculated based on the summed abundances of *G. bulloides, Neogloboquadrina dutertrei* and *Globigerinita glutinata*, which all thrive in high productivity surface waters, normalized to the summed abundance of all planktonic foraminiferal species.

435 **6.2.4 Planktonic foraminifera Mg/Ca measurements**

436 Mg/Ca analyses were performed in samples containing ca. 20 individuals
437 of *G. ruber pink* (250-350 μm) from the uppermost 236 cm of core M125-95-3,
438 which cover the last ca. 20 kyr. We followed the foraminiferal standard cleaning
439 protocol described in Barker et al. (2003) The cleaned *G. ruber* fragments were
440 analyzed with a Thermo Finnigan Element 2 sector field inductively coupled
441 plasma mass spectrometer (ICP-MS) at the Petrology of the Ocean Crust ICP-
442 MS Laboratory (Faculty of Geosciences, University of Bremen, Germany).
443 Exception was made for the interval between 92-194 cm which was analyzed
444 with an Agilent Technologies 700 series ICP optical emission spectrometer
445 (ICP-OES) with an ASX-520 Cetac autosampler and micro-nebulizer at the
446 MARUM – Center for Marine Environmental Sciences (University of Bremen,
447 Germany). Instrumental precision of ICP-MS and ICP-OES were monitored
448 through analyses of an in-house standard solution (which was the same for both
449 ICP-MS and ICP-OES) of theoretical value 3.40 mmol mol^{-1}. Mean long-term
450 standard deviation was 0.012 mmol mol^{-1}. The Al/Ca, Fe/Ca, and Mn/Ca ratios
451 were considered to monitor cleaning efficiency.

452 To convert Mg/Ca ratios into SSTs we applied the calibration proposed
453 by Gray and Evans (2019), which accounts for nonthermal effects (e.g., salinity
454 and carbonate chemistry). Since the currently available species-specific
455 calibration curves do not consider the *G. ruber* pink morphotype, we used the
456 *G. ruber* white morphotype curve. The uncertainties estimated for calibration
457 based on Mg/Ca SST values are within +/- 1.5 °C (Gray and Evans, 2019).
458

6.2.5 Benthic foraminiferal stable oxygen ($\delta^{18}O$)

Benthic foraminiferal $\delta^{18}O$ were measured on ~10 tests of *Cibicidoides wuellerstorfi* and/or *C. mundulus* for each sample of core SEAL-20230070. Analyses were performed with a Thermo Fisher Scientific MAT253 isotope ratio mass spectrometer coupled to a Kiel IV automated carbonate preparation device at the Paleoceanography and Paleoclimatology Laboratory (P2L), at University of São Paulo (USP), Brazil. Results are reported in permille (‰) deviation from the Vienna Pee Dee Belemnite (VPDB) scale. Standard deviation of repeated measurements of the in-house SHP2L standard (Crivellari et al., 2021) during the measurement period was <0.061‰.

6.2.6 Glycerol dialkyl glycerol tetraethers (GDGTs)

Between 2 to 3 g of dry and homogenized sediments were extracted using a modified Bligh and Dyer extraction procedure (Bligh and Dyer, 1959; Rütters et al., 2002). For this, the sediments were extracted in an ultrasonic bath using a solvent mixture of methanol (MeOH), dichloromethane (DCM) and phosphate buffer (2:1:0:8, v:v:v). After centrifugation, the supernatant was collected, and the residue extracted twice with the solvent mixture specified above. DCM and phosphate buffer were added to the pooled supernatants to achieve a ratio of MeOH/DCM/phosphate buffer of 1:1:0:9 (v:v:v), allowing the separation of two phases. The bottom layer, containing the organic fraction, was transferred to a round bottom flask and the remaining aqueous phase was

481 extracted twice with DCM. The combined extracts were reduced under rotary
482 vacuum, transferred to preweighed vials and dried under a gentle stream of N_2.
483 An aliquot of each Bligh and Dyer extract (~1 mg) was separated into
484 apolar and polar fractions using column chromatography. Al_2O_3 was used as
485 stationary phase, while hexane/DCM (9:1, v:v) and DCM/MeOH (1:1, v:v) were
486 used as respective eluents. The polar fractions, containing isoprenoid and
487 branched GDGTs, were dried under N_2, re-dissolved in hexane/2-propanol
488 (99:1, v:v) to a concentration of 2 mg/ml and filtered through a PFTE 0.45 µm
489 filter prior to analysis by high performance liquid chromatography/atmospheric
490 pressure chemical ionization-mass spectrometry (HPLC/APCI-MS) at the
491 Institute of Geosciences, University of Kiel, Germany.
492 Detection of GDGTs was achieved using a Waters Alliance 2695 high
493 performance liquid chromatograph (HPLC) coupled to a Micromass ZQ single
494 quadrupole mass spectrometer (MS). The HPLC was fitted with two Waters
495 BEH HILIC columns (2.1 × 150 mm, 1.7 µm) operated in tandem and a guard
496 column of the same material, which were maintained at 30 °C. The target
497 analytes were eluted with a flow rate of 0.2 mL min^{-1} and applying the gradient
498 profile reported by Hopmans et al., (2016).
499 The MS was equipped with an atmospheric pressure chemical ionization
500 interface (APCI) operated in positive ion mode. Source conditions were identical
501 to those provided in (Heyng et al., 2015). GDGTs were detected by selected ion
502 recording (SIR) of their $[M+H]^+$ ions (dwell time = 200 ms) according (Hopmans
503 et al., 2000; Hopmans et al., 2004). The TEX^H_{86} index was calculated and
504 transformed to SSTs as reported by Kim et al., (2010). The BIT index was

505 determined as defined by Hopmans et al., (2004) but using the combined peak
506 areas of 5- and 6-methyl brGDGT isomers.
507

508 **6.2.7 Age model**

509 The chronology of core SEAL-20230070 is based on five planktonic
510 foraminiferal accelerator mass spectrometry (AMS) ages. For each radiocarbon
511 sample, we handpicked between 450 and 700 *G. ruber* tests, which yielded
512 masses between 2.5 and 10 mg. Measurements were conducted at the Leibniz
513 Laboratory for Radiocarbon Dating and Stable Isotope Research (University of
514 Kiel, Germany) using a HVE 3MV Tandentron 4130 accelerator mass
515 spectrometer. Dating uncertainties account for the measured $^{14}C/^{13}C$ ratios of
516 samples and standards, as well as fractionation and blank corrections.
517 Radiocarbon ages were calibrated with the IntCal20 curve (Reimer et al.,
518 2020) with variable reservoir ages from the transient modelling experiments of
519 Butzin et al., (2017) in the software PaleoDataView version 0.9.5.5 (Langner
520 and Mulitza, 2019). We then derived a Bayesian age model for core SEAL-
521 20230070 using the BACON v. 2.2 age modelling tool (Blaauw and Christeny,
522 2011) wich was also done in PaleoDataView (v. 0.9.5.5). We followed the same
523 approach as Campos et al. (2019) for core M125-95-3, applying default
524 settings, except for mem.mean (set to 0.4), mem.strength (set to 4), and 10,000
525 realizations. All ages are reported as ka BP (present being 1950 AD).
526 Additionally, we updated the radiocarbon ages calibration from core M125-95-3
527 by using the IntCal20 curve (Reimer et al., 2020).

7. RESULTS

7.1 Core SEAL-20230070 chronology

Radiocarbon ages of the uppermost 190 cm of core SEAL-20230070 indicate that the sediment sequence covers the last ~20 kyr (Tab. 1; Fig. 2b), ranging from Marine Isotope Stage (MIS)2 to MIS1. Sedimentation rates of ~12 cm/kyr occurred between 20.2 to 13.5 ka BP, declined to ~7 cm/kyr between 13.5 and 2.9 ka BP, and reached ~22 cm/kyr between 2.9 and 1.4 ka BP (Fig. 2b). Our age estimates imply that the last 1.4 kyr BP were not recorded at core SEAL-20230070, which is in accordance with the age model proposed by Campos et al. (2019) for the nearby core M125-95-3.

Benthic foraminiferal $\delta^{18}O$ values ranges from 1.6 to 4.5‰ (Fig. 2a). The highest values (4.0 to 4.5‰) occurred at ~20 ka BP, whereas the lowest values (~2.0‰) occurred during the late Holocene. The overall trend and absolute values of the benthic foraminiferal $\delta^{18}O$ record agrees well with the $\delta^{18}O$ stack of (Lisiecki and Stern, 2016) for intermediate water depths in the Atlantic Ocean (Fig. 2a), providing independent evidence for the robustness of our age model. Benthic foraminiferal $\delta^{13}C$ values ranges from -0.044 to 2.025 (Fig. 3c), and presented relatively low values during HS1 and the YD.

552 Table 1: Accelerator mass spectrometer radiocarbon ages used to construct the
553 age model of core SEAL-202300070.

Sample depth (m)	Lab ID	Radiocarbon age ± 1s error (ka BP)	Calibrated median age (years)
0	KIA-55349	1,802 ± 0.025	1,394
0.35	KIA-55350	3,138 ± 0.026	2,957
0.75	KIA-553501	8,305 ± 0.035	8,826
1.1	KIA-553502	12,115 ± 0.055	13,540
1.9	KIA-553503	17,350 ± 0.120	20,203

554
555

556 **7.2 Continental runoff and hydroclimate proxies**

557 At core SEAL-20230070, the log(Ti/Ca) and log(Fe/Ca) ratios (Fig. 3e, f)
558 show marked increases within the HS1 chronozone. Both ratios decreased
559 during the Bølling-Allerød event (BA, 15-12.9 ka BP) and increase again during
560 the YD chronozone. Even though both HS1 and the YD were characterized by
561 positive excursions of the log(Ti/Ca) and log(Fe/Ca) ratios, maximum values
562 attained by both ratios were lower within the YD than within HS1. After the ~9.5
563 ka BP, log(Ti/Ca) and log(Fe/Ca) dropped markedly and recovered gradually
564 toward pre-HS values throughout the Holocene. The Log(Fe/K) ratio also
565 displays positive excursions within HS1, the YD (until ~9.5 ka BP) and, to a
566 lesser extent, after ~3 ka BP (Fig. 3d). Log(Fe/K) show low values within the BA
567 and between 9 and 3 ka BP (Fig. 3d). Increased log(Ti/Ca), log(Fe/Ca) and
568 log(Fe/K) (Fig. 3d-f) persist for ~2 kyr after the YD.

569 Brightness (L*) (Fig. 3c) shows an opposite trend compared to those
570 depicted by the log(Ti/Ca), log(Fe/Ca) and log(Fe/K) ratios. Lighter tones
571 (values close to or above 0.9) mark the last glacial maximum (LGM), the BA
572 event and the interval between 9 and 3 ka BP, whereas darker tones (values
573 below 0.9) characterize sediments deposited during HS1, the YD and after 3 ka
574 BP.

575 BIT values (Fig.3) range from 0.82 at the base of the studied interval to
576 0.25 at the core top. They were the highest (above 0.70) during MIS2 and
577 showed a stepwise decrease over time. The first decrease occurred during the
578 BA, where the BIT index declines to an average value of 0.55 (Fig. 3a). The
579 second decrease took place at ~9.5 ka BP. Throughout the Holocene, BIT
580 values varied from 0.25 to 0.39 (average of 0.31±0.05).

581 **7.3 Paleoproductivity proxies**

582 Total abundance of planktonic foraminifera at core SEAL-20230070
583 varied between 4 and 1497 specimens/g of sediment (Fig. 4g). Values were the
584 lowest during HS1 and between 12 and 10 ka BP. They increased markedly
585 during the BA event and at ~9.5 ka BP. *G. ruber* is the most abundant species
586 (Fig 4e), with relative abundances varying from 40 to 78%. The lowest
587 percentages of *G. ruber* (40%) occurred during HS1, followed by a marked
588 recovery at the onset of the BA (Fig. 4e).

589 Relative abundances of *G. bulloides* ranged from 0 to 4%, with the
590 highest percentages occurring during HS1 and the YD events (Fig. 4b). A
591 similar trend is depicted by the combined relative abundances of *T. trilobus* and
592 *T. sacculifer*, which ranged from 1.6 to 23%, with highest percentages during

593 HS1, but also showing a significant increase during the YD chronozone (Fig.
594 4c). Relative abundances of *G. bulloides* and *T. trilobus* + *T. sacculifer*
595 remained low throughout the Holocene. Values of the $R_{HP/Planktonic}$ index
596 remained low (on average ~0.7) throughout the studied sequence, except
597 during HS1, when values peaked above 1.0 (Fig. 4d).

598 **7.4 Sea surface temperature (SST) proxies**

599 TEX^{H}_{86} results from core SEAL-20230070 indicates that SSTs remained
600 high (around 27 °C) during HS1 (Fig. 4h). During the BA, SST dropped to 24.5
601 ºC. Within the YD, SST ranged from 25 °C to 27 °C. The highest SSTs were
602 recorded after the YD, at ~10 kyr BP, when they peaked at almost 29 °C.
603 Between ~8 and ~2 ka BP, SSTs remained relatively constant between 25.5 C°
604 and 26.5 °C.

605 Reconstructed SSTs from nearby core M125-95-3, based on planktonic
606 foraminiferal Mg/Ca paleothermometry indicate that SSTs ranged from 26 °C to
607 28 °C during HS1 (Fig. 4h). Within the BA SSTs oscillated between 26 °C and
608 27.5 °C, while they dropped to ~26 °C during the YD and showed a minimum of
609 (25.2 °C) at ~5.8 ka BP.

610

611 **8. DISCUSSION**

612 **8.1 Hydroclimate records from tropical South America**

613 Geochemical proxy data from tropical marine paleoclimate records
614 collected from the Atlantic South American continental margin indicate
615 precipitation anomalies during HS1 and the YD chronozones (Fig. 5b). There is

616 evidence of precipitation anomalies over northern (Bahr et al., 2018; Haug et
617 al., 2001) northwestern (Crivellari et al., 2018; Zhang et al., 2017) and
618 northeastern (Arz et al., 1998; Mulitza et al., 2017) South America. This
619 included evidence for negative precipitation anomalies and relatively dry climate
620 conditions over northern (e.g., Bahr et al., 2018; Haug et al., 2001) and
621 northwestern South America (e.g., Crivellari et al., 2018; Zhang et al., 2017),
622 while the northeastern regions were characterized by positive precipitation
623 anomalies and significantly wetter conditions (e.g., Arz et al., 1998; Mulitza et
624 al., 2017)

625 Our paleoclimate records are in line with previous hydroclimate/runoff
626 reconstruction over northeastern South America (Arz et al., 1998; Campos et
627 al., 2019; Mulitza et al., 2017; Stríkis et al., 2018, 2015), since marked
628 increases in continental runoff from the São Francisco River drainage basin to
629 the location of core SEAL-20230070 were depicted by the BIT, log(Ti/Ca),
630 log(Fe/Ca) and L* records during HS1 and the YD (Fig. 3). The increase in
631 terrigenous supply also diluted planktonic foraminiferal absolute abundances
632 (specimens/g) which significantly declined during HS1 and the YD. Our
633 log(Fe/K) record suggests that chemical weathering over eastern tropical South
634 America was also enhanced during HS1 and the YD. This interpretation is
635 supported by stalagmite $\delta^{18}O$ records from eastern Brazil (Stríkis et al., 2018)
636 that suggest an increase in the amount of rainfall during HS1 and the YD,
637 interrupted by a decrease in rainfall during the BA.

638 An austral summer intensification of the SACZ during HS1 was
639 suggested by Stríkis et al. (2015) to explain these positive precipitation
640 anomalies over eastern Brazil. However, Campos et al. (2019), suggested,

641 based on proxy and modeling data, that austral summers during HS1 were
642 characterized by decreased precipitation in vast regions of tropical South
643 America, including most of the Amazon River drainage basin and the northern
644 Parnaíba River drainage basin. This dry anomaly was attributed mainly to
645 relatively colder and drier air masses transported from the North Atlantic
646 towards South America (Campos et al., 2019). Eastern South America between
647 ca. 15°S and 25°S, however, experienced an increase in austral summer
648 precipitation, which was likely associated with an anomalous cyclonic circulation
649 and humidity transport from a relatively warmer South Atlantic towards the
650 continent (Campos et al., 2019). This hypothesis is supported by SST warming
651 following the LGM in western tropical South Atlantic Ocean, as depicted by both
652 Mg/Ca and TEX^{H}_{86} paleothermometers during the HS1 (Fig. 4), with values
653 close to present-day SSTs (Fig. 1). According to modelling results by Campos
654 et al. (2019), increased continental runoff and chemical weathering intensity,
655 depicted by our BIT, log(Ti/Ca), log(Fe/Ca), log(Fe/K) and L* records, were
656 likely related to an increase in precipitation upstream in the São Francisco River
657 drainage basin (close to 20°S, Fig. 1).

658 For the YD, positive continental runoff anomalies and intensified
659 chemical weathering (high log(Ti/Ca), log(Fe/Ca), log(Fe/K) and BIT) at core
660 SEAI-20230070 persisted for ~2 kyr after the event (Fig. 3). This pattern could
661 be related to the low resolution of our age model, since there are no
662 radiocarbon ages bracketing the event until ca. 8.6 ka BP (Tab. 1; Fig. 2).
663 However, we noticed that the nearby core M125-95-3 (Campos et al., 2019)
664 depicted comparable high ln(Ti/Ca) and ln(Fe/K) until ~9.5 ka BP (Fig. 5e, g).
665 This remarkable resemblance of the elemental records at cores SEAI-20230070

666 and M125-95-3 suggest that increased log(Ti/Ca), log(Fe/Ca), log(Fe/K) and
667 BIT until ~9.5 ka BP are not an age model bias, but instead reocord an
668 environmental signal. In fact, continental runoff maxima centerd at ~10 ka BP
669 were reported for marine cores collected on the western Australia margin
670 (Kuhnt et al., 2015) as a response to intensification of the Australian monsoon
671 system. The similarity of continetal runnoff records located on the northeastern
672 South America and western Australian margins during HS1, the YD and at ~10
673 ka BP, points to synchrous shifts in precipitation patterns in the Southern
674 Hemisphere, as a response to milenial-scale deglatial climate change.

675 **8.2 Coupling between atmospheric and oceanic processes**

676 Even though both HS1 and the YD were characterized by high BIT,
677 log(Ti/Ca), log(Fe/Ca) and log(Fe/K) at core SEAL-20230070, the amplitudes of
678 positive log(Ti/Ca) and log(Fe/Ca) excursions were larger during HS1 (Fig. 3).
679 This pattern suggests that precipitation and continental runoff were more
680 intense during HS1 compared to the YD. During these events, the AMOC was
681 nearly collapsed and weakened, respectively, as suggested by $^{231}Pa/^{230}Th$
682 records (Fig. 3b) (McManus et al., 2004), and supported by low $\delta^{13}C$ values at
683 core SEAL-20230070 (Fig. 3c). Under the present climate state, a strong AMOC
684 promotes oceanic transport of heat from the Southern to the Northern
685 Hemisphere (Buckley and Marshall, 2016; Ganachaud and Wunsch, 2000). To
686 compensate for this inter-hemispheric asymmetry, atmospheric cross-equatorial
687 net energy transport is directed towards the Southern Hemisphere (Marshall et
688 al., 2014). Thus, the location of the ascending branch of the Hadley cell (e.g.,
689 the ITCZ) is presently located north of the Equator. Since AMOC almost

690 collapsed or weakened during HS1 and the YD (Mohtadi et al., 2016; Zhang et
691 al., 2017), oceanic heat transport to the Northern Hemisphere and the reversed
692 cross-equatorial atmospheric energy transport were reduced. As a result, the
693 ITCZ shifted southward and strongly impacted the climate of South America
694 (e.g., Mohtadi et al., 2016; Mulitza et al., 2017; Campos et al., 2019; Venancio
695 et al., 2020b)

696 During periods of slow AMOC, the decreased heat transport to the North
697 Atlantic would trap heat in the Southern Hemisphere (e.g., Broecker, 1998;
698 Chiessi et al., 2015). Therefore, the Brazil Current (BC) surface layer acted as a
699 storage for some of the heat that was not transported to the North Atlantic
700 during HS1 (Chiessi et al., 2015; Meier et al., 2021). Our new SST records of
701 the western tropical South Atlantic support this finding by showing close to
702 present day SSTs at the sites of cores SEAL-20230070 and M125-95-3 during
703 HS1 and the YD (Fig. 4h), the latter warm temperatures depicted only by the
704 TEX^{H}_{86} record.

705 As a note of caution, we cannot rule out an influence of deglacial sea
706 level rise (e.g., Fairbanks, 1989; Miller et al., 2020) on the different amplitudes
707 of the positive log(Ti/Ca) and log(Fe/Ca) excursions at core SEAL-20230070
708 during HS1 and the YD. Indeed, a higher sea level during the YD in relation to
709 HS1 would have shifted the coastline further inland, decreasing the input of
710 terrigenous sediments to our core sites. However, when we remove the long-
711 term linear trend from the log(Ti/Ca) and log(Fe/Ca) records at core SEAL-
712 2023, the amplitudes of the HS1 positive excursions are still higher than the
713 ones during the YD and lasting until 9.5 ka BP (Fig. 6). Additionally, deglacial
714 changes in sea level alone are unlikely to explain the distinct behavior of

715 paleoproductivity between both millennial-scale events of the last deglaciation
716 (see section 6.3).
717

718 **8.3 Paleoproductivity and water column stratification**

719 Our data indicate an increase in primary productivity during HS1 in the
720 western tropical South Atlantic (Fig. 4d). This is supported by increased
721 abundances of *G. bulloides* during HS1 at core SEAL-20230070 (Fig. 4b),
722 coupled with decreased abundances of the symbiont-bearing oligotrophic
723 species *G. ruber* (Fig. 4e). Indeed, *G. bulloides* generally inhabits relatively cold
724 and nutrient-rich waters (e.g., Portilho-Ramos et al., 2019; de Oliveira Lessa et
725 al., 2014; Mohtadi et al., 2007). These changes in the abundance of planktonic
726 foraminiferal species occurred in tandem with an increase of the $R_{HP/Planktonic}$
727 index during HS1 (Fig. 4d), which is also indicative of a relative increase in
728 surface ocean productivity. During the YD, relative abundances of *G. bulloides*
729 also increased; however, the $R_{HP/Planktonic}$ index remained low, and *G. ruber*
730 relative abundances increased in relation to HS1 values (Fig. 4). These
731 observations imply that surface productivity was higher during HS1 that during
732 the YD in the western tropical South Atlantic.
733 We consider it unlikely that increased productivity during HS1 was
734 related to intensified upwelling of nutrient-rich cold waters. In fact, TEX^{H}_{86} and
735 Mg/Ca paleothermometers from cores SEAL-20230070 and M125-95-3 indicate
736 high, close to modern, SSTs during HS1 (Fig. 4h).
737 Taken together, our results suggest that an increased supply of nutrients
738 by continental runoff boosted primary productivity during HS1 in the western

739 tropical South Atlantic. This mechanism may enable to explain the different
740 surface productivity responses during HS1, and the YD observed at core SEAL-
741 20230070: A nearly-collapsed AMOC state during HS1 caused a marked
742 increase in precipitation over northeastern tropical South America and in the
743 supply of nutrient to our core location, whereas a weak AMOC state (with likely
744 less intense precipitation) during the YD did not allow for a significantly increase
745 in primary productivity. Additionally, deglacial sea level rise also shifted inland
746 the mouth of the São Francisco River, moving the source of nutrients farther
747 away from our core location during the YD, in comparison with the HS1 setting.
748 This role of continental runoff in sustaining primary productivity also explains the
749 higher $R_{HP/Planktonic}$ values during HS1 at core SEAL-2023007, which is located
750 closer to the continent, than the $R_{HP/Planktonic}$ values at the more distal (and
751 deeper) core M125-95-3 (Campos et al., 2020).
752

753 **9. CONCLUSIONS**

754 We present new data for sediment cores SEAL-20230070 and M125-95-
755 3, increasing the coverage of marine paleoclimate records spanning the last 20
756 kyr in the western tropical South Atlantic, off eastern tropical South America.
757 Our data indicate positive precipitation anomalies over the São Francisco River
758 drainage basin during HS1 and from the YD until ~9.5 ka BP, and relatively dry
759 conditions during the BA event. The most pronounced increases in precipitation
760 and continental runoff likely occurred during HS1, when AMOC almost
761 collapsed, whereas positive anomalies of both parameters were weaker during
762 the YD, when AMOC intensity was only reduced. Together with previous
763 studies, our SST reconstructions suggest that heat trapped in the western

764 tropical South Atlantic, under a less intense AMOC, was fundamental in
765 controlling increases in precipitation over northeastern tropical South America.
766 Additionally, we propose that enhanced surface productivity in the western
767 tropical South Atlantic during HS1 was likely controlled by increased input of
768 nutrients by continental runoff, related to positive precipitation anomalies
769

770 **ACKNOWLEDGEMENTS**

771 The core was collected in 2000 and donated to itt Fossil (UNISINOS) by
772 the National Petroleum Agency (ANP) of Brazil. We thank G.E.R. Racolte for
773 assistance during spectral analysis, using the spectroradiometer provided by
774 VizLab (UNISINOS University); J.P.Z. Gomes for assistance with spectral
775 reflectance and XRF analyses; and H.J.H. Johnstone for assistance with ICP-
776 OES analyses.
777

778 **Funding Sources**

779 K.G.D.K. received financial support by the National Council of Scientific and
780 Technologic Development (CNPq grant 409705-2018-7). C.M.C. acknowledges
781 the financial support from FAPESP (grants 2018/15123-4 and 2019/24349-9),
782 CAPES (grant 88881.313535/201901), CNPq (grant 312458/2020-7) and the
783 Alexander von Humboldt Foundation. M.C.C. acknowledges the financial
784 support from FAPESP (grants 2016/10242-0, 2018/06790-7 and 2019/25179-0).
785
786
787
788

Data availability

All new data collected in this study will be made available at the PANGAEA Data Publisher for Earth and Environmental Science (https://www.pangaea.de). Planktonic foraminiferal census counts were performed as part of the Bachelor Thesis by T. N. Zardin and also made available at PANGAEA.

Author's contributions

Alisson K. Martins: Conceptualization, Methodology, Validation, Investigation, Data Curation, Writing - Original Draft, Writing - Review & Editing, Visualization. **Karlos G. D. Kochhann:** Conceptualization, Methodology, Validation, Writing - Original Draft, Writing - Review & Editing, Visualization, Supervision, Project administration. **Cristiano M. Chiessi:** Methodology, Validation, Writing - Original Draft, Writing - Review & Editing, Visualization, Supervision, Project administration. **Thorsten Bauersachs:** Writing - Review & Editing, Methodology, Investigation, Data Curation. **Tamires N. Zardin:** Writing - Review & Editing, Methodology, Investigation, Data Curation. **Marília C. Campos:** Writing - Review & Editing, Methodology, Investigation, Data Curation. **Guilherme Krahl:** Methodology, Investigation, Data Curation. **Laís V de Souza:** Methodology, Investigation, Data Curation. **Stefano Crivellari:** Methodology, Investigation, Data Curation. **André Bahr:** Methodology, Investigation, Data Curation, Writing - Review & Editing, Visualization. **Henning Kuhnert:** Methodology, Investigation, Data Curation, Writing - Review & Editing, Visualization. **Lorenz Schwark:** Methodology, Investigation, Data Curation, Writing - Review & Editing, Visualization. **Gerson Fauth:** Conceptualization, Methodology, Validation, Writing - Review & Editing, Visualization, Supervision, Project administration.

819 **REFERENCES**

820 Arz, H.W., Pätzold, J., Wefer, G., 1998. Correlated millennial-scale changes in
821 surface hydrography and terrigenous sediment yield inferred from Last-
822 Glacial marine deposits off northeastern Brazil. Quat. Res. 50, 157–166.
823 https://doi.org/10.1006/qres.1998.1992
824 Bahr, A., Hoffmann, J., Schönfeld, J., Schmidt, M.W., Nürnberg, D., Batenburg,
825 S.J., Voigt, S., 2018. Low-latitude expressions of high-latitude forcing
826 during Heinrich Stadial 1 and the Younger Dryas in northern South
827 America. Glob. Planet. Change 160, 1–9.
828 https://doi.org/10.1016/J.GLOPLACHA.2017.11.008
829 Balsam, W.L., Deaton, B.C., Damuth, J.E., 1999. Evaluating optical lightness as
830 a proxy for carbonate content in marine sediment cores. Mar. Geol. 161,
831 141–153. https://doi.org/10.1016/S0025-3227(99)00037-7
832 Bard, E., Rostek, F., Turon JL, Gendreau S, 2000. Hydrological impact of
833 heinrich events in the subtropical northeast atlantic. Science 289, 1321–
834 1324. https://doi.org/10.1126/SCIENCE.289.5483.1321
835 Barker, S., Diz, P., Vautravers, M.J., Pike, J., Knorr, G., Hall, I.R., Broecker,
836 W.S., 2009. Interhemispheric Atlantic seesaw response during the last
837 deglaciation. Nature 457, 1097–1102. https://doi.org/10.1038/nature07770
838 Barker, S., Greaves, M., Elderfield, H., 2003. A study of cleaning procedures
839 used for foraminiferal Mg/Ca paleothermometry. Geochemistry, Geophys.
840 Geosystems 4, 1–20. https://doi.org/10.1029/2003GC000559
841 Blaauw, M., Christeny, J.A., 2011. Flexible paleoclimate age-depth models
842 using an autoregressive gamma process. Bayesian Anal. 6, 457–474.
843 https://doi.org/10.1214/11-BA618

844 Bligh, E.G., Dyer, W.J., 1959. A rapid method of total lipid extraction and
845 purification. Can. J. Biochem. Physiol. 37, 911–917.
846 https://doi.org/10.1139/O59-099
847 Bond, G., Heinrich, H., Broecker, W., Labeyrie, L., McManus, J., Andrews, J.,
848 Huon, S., Jantschik, R., Clasen, S., Simet, C., Tedesco, K., Klas, M.,
849 Bonani, G., Ivy, S., 1992. Evidence for massive discharges of icebergs into
850 the North Atlantic ocean during the last glacial period. Nat. 1992 3606401
851 360, 245–249. https://doi.org/10.1038/360245a0
852 Broecker, W.S., 1998. Paleocean circulation during the Last Deglaciation: A
853 bipolar seesaw? Paleoceanography 13, 119–121.
854 https://doi.org/10.1029/97PA03707
855 Broecker, W.S., 1994. Massive iceberg discharges as triggers for global climate
856 change. Nat. 1994 3726505 372, 421–424.
857 https://doi.org/10.1038/372421a0
858 Buckley, M.W., Marshall, J., 2016. Observations, inferences, and mechanisms
859 of the Atlantic Meridional Overturning Circulation: A review. Rev. Geophys.
860 54, 5–63. https://doi.org/10.1002/2015RG000493
861 Butzin, M., Köhler, P., Lohmann, G., 2017. Marine radiocarbon reservoir age
862 simulations for the past 50,000 years. Geophys. Res. Lett. 44, 8473–8480.
863 https://doi.org/10.1002/2017GL074688
864 Calvert, S.E., Pedersen, T.F., 2007. Chapter Fourteen Elemental Proxies for
865 Palaeoclimatic and Palaeoceanographic Variability in Marine Sediments:
866 Interpretation and Application. Dev. Mar. Geol. 1, 567–644.
867 https://doi.org/10.1016/S1572-5480(07)01019-6
868 Campos, M.C., Chiessi, C.M., Prange, M., Mulitza, S., Kuhnert, H., Paul, A.,

869 Venancio, I.M., Albuquerque, A.L.S., Cruz, F.W., Bahr, A., 2019. A new
870 mechanism for millennial scale positive precipitation anomalies over
871 tropical South America. Quat. Sci. Rev. 225.
872 https://doi.org/10.1016/j.quascirev.2019.105990
873 Chiessi, C.M., Mulitza, S., Mollenhauer, G., Silva, J.B., Groeneveld, J., Prange,
874 M., 2015. Thermal evolution of the western South Atlantic and the adjacent
875 continent during Termination 1. Clim. Past 11, 915–929.
876 https://doi.org/10.5194/CP-11-915-2015
877 Crivellari, S., Chiessi, C.M., Kuhnert, H., Häggi, C., da Costa Portilho-Ramos,
878 R., Zeng, J.Y., Zhang, Y., Schefuß, E., Mollenhauer, G., Hefter, J.,
879 Alexandre, F., Sampaio, G., Mulitza, S., 2018. Increased Amazon
880 freshwater discharge during late Heinrich Stadial 1. Quat. Sci. Rev. 181,
881 144–155. https://doi.org/10.1016/j.quascirev.2017.12.005
882 de Oliveira Lessa, D.V., Ramos, R.P., Barbosa, C.F., da Silva, A.R., Belem, A.,
883 Turcq, B., Albuquerque, A.L., 2014. Planktonic foraminifera in the sediment
884 of a western boundary upwelling system off Cabo Frio, Brazil. Mar.
885 Micropaleontol. 106, 55–68.
886 https://doi.org/10.1016/J.MARMICRO.2013.12.003
887 Fairbanks, R.G., 1989. A 17,000-year glacio-eustatic sea level record: influence
888 of glacial melting rates on the Younger Dryas event and deep-ocean
889 circulation. Nat. 1989 3426250 342, 637–642.
890 https://doi.org/10.1038/342637a0
891 Firestone, R.B., West, A., Kennett, J.P., Becker, L., Bunch, T.E., Revay, Z.S.,
892 Schultz, P.H., Belgya, T., Kennett, D.J., Erlandson, J.M., Dickenson, O.J.,
893 Goodyear, A.C., Harris, R.S., Howard, G.A., Kloosterman, J.B., Lechler, P.,

894 Mayewski, P.A., Montgomery, J., Poreda, R., Darrah, T., Que Hee, S.S.,
895 Smitha, A.R., Stich, A., Topping, W., Wittke, J.H., Wolbach, W.S., 2007.
896 Evidence for an extraterrestrial impact 12,900 years ago that contributed to
897 the megafaunal extinctions and the Younger Dryas cooling. Proc. Natl.
898 Acad. Sci. U. S. A. 104, 16016–16021.
899 https://doi.org/10.1073/pnas.0706977104
900 Ganachaud, A., Wunsch, C., 2000. Improved estimates of global ocean
901 circulation, heat transport and mixing from hydrographic data. Nature 408,
902 453–457. https://doi.org/10.1038/35044048
903 Govin, A., Holzwarth, U., Heslop, D., Keeling, L.F., Zabel, M., Mulitza, S.,
904 Collins, J.A., Chiessi, C.M., 2012. Distribution of major elements in Atlantic
905 surface sediments (36°N–49°S): Imprint of terrigenous input and
906 continental weathering. Geochemistry, Geophys. Geosystems 13.
907 https://doi.org/10.1029/2011GC003785
908 Gray, W.R., Evans, D., 2019. Nonthermal Influences on Mg/Ca in Planktonic
909 Foraminifera: A Review of Culture Studies and Application to the Last
910 Glacial Maximum. Paleoceanogr. Paleoclimatology 34, 306–315.
911 https://doi.org/10.1029/2018PA003517
912 Haug, G.H., Hughen, K.A., Sigman, D.M., Peterson, L.C., Röhl, U., 2001.
913 Southward migration of the intertropical convergence zone through the
914 holocene. Science (80-.). 293, 1304–1308.
915 https://doi.org/10.1126/SCIENCE.1059725
916 Heinrich, H., 1988. Origin and Consequences of Cyclic Ice Rafting in the
917 Northeast Atlantic Ocean During the Past 130,000 Years. Quat. Res. 29,
918 142–152. https://doi.org/10.1016/0033-5894(88)90057-9

Heyng, A.M., Mayr, C., Lücke, A., Moschen, R., Wissel, H., Striewski, B., Bauersachs, T., 2015. Middle and Late Holocene paleotemperatures reconstructed from oxygen isotopes and GDGTs of sediments from Lake Pupuke, New Zealand. Quat. Int. 374, 3–14. https://doi.org/10.1016/J.QUAINT.2014.12.040

Holtvoeth, J., Wagner, T., Schubert, C.J., 2003. Organic matter in river-influenced continental margin sediments: The land-ocean and climate linkage at the Late Quaternary Congo fan (ODP Site 1075). Geochemistry, Geophys. Geosystems 4. https://doi.org/10.1029/2003GC000590

Hopmans, E.C., Schouten, S., Pancost, R.D., Van Der Meer, M.T.J., Sinninghe Damsté, J.S., 2000. Analysis of intact tetraether lipids in archaeal cell material and sediments by high performance liquid chromatography/atmospheric pressure chemical ionization mass spectrometry. Rapid Commun. Mass Spectrom. 14, 585–589. https://doi.org/10.1002/(SICI)1097-0231(20000415)14:7<585::AID-RCM913>3.0.CO;2-N

Hopmans, E.C., Schouten, S., Sinninghe Damsté, J.S., 2016. The effect of improved chromatography on GDGT-based palaeoproxies. Org. Geochem. 93, 1–6. https://doi.org/10.1016/J.ORGGEOCHEM.2015.12.006

Hopmans, Ellen C., Weijers, J.W.H., Schefuß, E., Herfort, L., Sinninghe Damsté, J.S., Schouten, S., 2004. A novel proxy for terrestrial organic matter in sediments based on branched and isoprenoid tetraether lipids. Earth Planet. Sci. Lett. 224, 107–116. https://doi.org/10.1016/J.EPSL.2004.05.012

Hopmans, E. C., Weijers, J.W.H., Schefuß, E., Herfort, L., Sinninghe Damsté,

J.S., Schouten, S., 2004. A novel proxy for terrestrial organic matter in sediments based on branched and isoprenoid tetraether lipids. Earth Planet. Sci. Lett. 224, 107–116. https://doi.org/10.1016/j.epsl.2004.05.012

Kageyama, M., Merkel, U., Otto-Bliesner, B., Prange, M., Abe-Ouchi, A., Lohmann, G., Ohgaito, R., Roche, D.M., Singarayer, J., Swingedouw, D., 2013. Climatic impacts of fresh water hosing under Last Glacial Maximum conditions: a multi-model study. Clim. Past 9, 935–953. https://doi.org/10.5194/cp-9-935-2013

Kim, J.H., van der Meer, J., Schouten, S., Helmke, P., Willmott, V., Sangiorgi, F., Koç, N., Hopmans, E.C., Damsté, J.S.S., 2010. New indices and calibrations derived from the distribution of crenarchaeal isoprenoid tetraether lipids: Implications for past sea surface temperature reconstructions. Geochim. Cosmochim. Acta 74, 4639–4654. https://doi.org/10.1016/J.GCA.2010.05.027

Kuhnt, W., Holbourn, A., Xu, J., Opdyke, B., De Deckker, P., Röhl, U., Mudelsee, M., 2015. Southern Hemisphere control on Australian monsoon variability during the late deglaciation and Holocene. Nat. Commun. 6. https://doi.org/10.1038/ncomms6916

Langner, M., Mulitza, S., 2019. PaleoDataView (PDV) – User Guide.

Li, M., Hinnov, L., Kump, L., 2019. Acycle: Time-series analysis software for paleoclimate research and education. Comput. Geosci. 127, 12–22. https://doi.org/10.1016/J.CAGEO.2019.02.011

Lisiecki, L.E., Stern, J. V., 2016. Regional and global benthic δ18O stacks for the last glacial cycle. Paleoceanography 31, 1368–1394. https://doi.org/10.1002/2016PA003002

969 Locarnini, R.A., Mishonov, J.I.A., Boyer, T.P., Garcia, H., Baranova, O.K.,
970 Zweng, M.M., Paver, C.R., Reagan, J.R., Johnson, D.R., Hamilton, M.,
971 Seidov, D., 2013. World Ocean Atlas 2013, Volume 1: Temperature. NOAA
972 Atlas NESDIS 1, 40. https://doi.org/10.7289/V55X26VD
973 Marshall, J., Donohoe, A., Ferreira, D., McGee, D., 2014. The ocean's role in
974 setting the mean position of the Inter-Tropical Convergence Zone. Clim.
975 Dyn. 42, 1967–1979. https://doi.org/10.1007/S00382-013-1767-Z
976 McManus, J.F., Francois, R., Gherardi, J.-M., Keigwin, L.D., Brown-Leger, S.,
977 2004. Collapse and rapid resumption of Atlantic meridional circulation
978 linked to deglacial climate changes. Nat. 2004 4286985 428, 834–837.
979 https://doi.org/10.1038/nature02494
980 Meier, K.J.F., Bahr, A., Chiessi, C.M., Albuquerque, A.L., Raddatz, J., Friedrich,
981 O., 2021. Role of the Tropical Atlantic for the Interhemispheric Heat
982 Transport During the Last Deglaciation. Paleoceanogr. Paleoclimatology
983 36. https://doi.org/10.1029/2020PA004107
984 Miller, K.G., Browning, J. V., John Schmelz, W., Kopp, R.E., Mountain, G.S.,
985 Wright, J.D., 2020. Cenozoic sea-level and cryospheric evolution from
986 deep-sea geochemical and continental margin records. Sci. Adv. 6.
987 https://doi.org/10.1126/sciadv.aaz1346
988 Mohtadi, M., Max, L., Hebbeln, D., Baumgart, A., Krück, N., Jennerjahn, T.,
989 2007. Modern environmental conditions recorded in surface sediment
990 samples off W and SW Indonesia: Planktonic foraminifera and biogenic
991 compounds analyses. Mar. Micropaleontol. 65, 96–112.
992 https://doi.org/10.1016/J.MARMICRO.2007.06.004
993 Mohtadi, M., Prange, M., Steinke, S., 2016. Palaeoclimatic insights into forcing

994 and response of monsoon rainfall. Nature 533, 191–199.
995 https://doi.org/10.1038/nature17450
996 Mulitza, S., Chiessi, C.M., Schefuß, E., Lippold, J., Wichmann, D., Antz, B.,
997 Mackensen, A., Paul, A., Prange, M., Rehfeld, K., Werner, M., Bickert, T.,
998 Frank, N., Kuhnert, H., Lynch-Stieglitz, J., Portilho-Ramos, R.C.,
999 Sawakuchi, A.O., Schulz, M., Schwenk, T., Tiedemann, R., Vahlenkamp,
1000 M., Zhang, Y., 2017. Synchronous and proportional deglacial changes in
1001 Atlantic meridional overturning and northeast Brazilian precipitation.
1002 Paleoceanography 32, 622–633. https://doi.org/10.1002/2017PA003084
1003 Pinho, T.M.L., Chiessi, C.M., Portilho-Ramos, R.C., Campos, M.C., Crivellari,
1004 S., Nascimento, R.A., Albuquerque, A.L.S., Bahr, A., Mulitza, S., 2021.
1005 Meridional changes in the South Atlantic Subtropical Gyre during Heinrich
1006 Stadials. Sci. Rep. 11, 1–10. https://doi.org/10.1038/s41598-021-88817-0
1007 Portilho-Ramos, R., Pinho, T.M.L., Chiessi, C.M., Barbosa, C.F., 2019.
1008 Understanding the mechanisms behind high glacial productivity in the
1009 southern Brazilian margin. Clim. Past 15, 943–955.
1010 https://doi.org/10.5194/CP-15-943-2019
1011 Portilho-Ramos, R.C., Chiessi, C.M., Zhang, Y., Mulitza, S., Kucera, M., Siccha,
1012 M., Prange, M., Paul, A., 2017. Coupling of equatorial Atlantic surface
1013 stratification to glacial shifts in the tropical rainbelt. Sci. Rep. 7, 1–8.
1014 https://doi.org/10.1038/s41598-017-01629-z
1015 Reimer, P.J., Austin, W.E.N., Bard, E., Bayliss, A., Blackwell, P.G., Bronk
1016 Ramsey, C., Butzin, M., Cheng, H., Edwards, R.L., Friedrich, M., Grootes,
1017 P.M., Guilderson, T.P., Hajdas, I., Heaton, T.J., Hogg, A.G., Hughen, K.A.,
1018 Kromer, B., Manning, S.W., Muscheler, R., Palmer, J.G., Pearson, C., Van

1019 Der Plicht, J., Reimer, R.W., Richards, D.A., Scott, E.M., Southon, J.R.,
1020 Turney, C.S.M., Wacker, L., Adolphi, F., Büntgen, U., Capano, M., Fahrni,
1021 S.M., Fogtmann-Schulz, A., Friedrich, R., Köhler, P., Kudsk, S., Miyake, F.,
1022 Olsen, J., Reinig, F., Sakamoto, M., Sookdeo, A., Talamo, S., 2020. The
1023 IntCal20 Northern Hemisphere Radiocarbon Age Calibration Curve (0-55
1024 cal kBP). Radiocarbon 62, 725–757. https://doi.org/10.1017/RDC.2020.41
1025 Renssen, H., Mairesse, A., Goosse, H., Mathiot, P., Heiri, O., Roche, D.M.,
1026 Nisancioglu, K.H., Valdes, P.J., 2015. Multiple causes of the Younger
1027 Dryas cold period. Nat. Geosci. 8, 946–949.
1028 https://doi.org/10.1038/ngeo2557
1029 Rütters, H., Sass, H., Cypionka, H., Rullkötter, J., 2002. Phospholipid analysis
1030 as a tool to study complex microbial communities in marine sediments. J.
1031 Microbiol. Methods 48, 149–160. https://doi.org/10.1016/S0167-
1032 7012(01)00319-0
1033 Schneider, R.R., Price, B., Müller, P.J., Kroon, D., Alexander, I., 1997. Monsoon
1034 related variations in Zaire (Congo) sediment load and influence of fluvial
1035 silicate supply on marine productivity in the east equatorial Atlantic during
1036 the last 200,000 years. Paleoceanography 12, 463–481.
1037 https://doi.org/10.1029/96PA03640
1038 Schlitzer, R. Ocean Data View. http://odv.awi.de (2016).
1039 Stefano Crivellari, Junia Viana, P., Carvalho Campos, M. de, Henning Kuhnert,
1040 Lopes, A.B.M., da Cruz, F.W., Mazur Chiessi, C., 2021. Development and
1041 characterization of a new in-house reference material for stable carbon and
1042 oxygen isotopes analyses. J. Anal. At. Spectrom. 36, 1125–1134.
1043 https://doi.org/10.1039/D1JA00030F

1044 Stramma, L., England, M., 1999. On the water masses and mean circulation of
1045 the South Atlantic Ocean. J. Geophys. Res. Ocean. 104.
1046 https://doi.org/10.1029/1999jc900139
1047 Stríkis, N.M., Chiessi, C.M., Cruz, F.W., Vuille, M., Cheng, H., De Souza
1048 Barreto, E.A., Mollenhauer, G., Kasten, S., Karmann, I., Edwards, R.L.,
1049 Bernal, J.P., Sales, H.D.R., 2015. Timing and structure of Mega-SACZ
1050 events during Heinrich Stadial 1. Geophys. Res. Lett. 42, 5477–5484.
1051 https://doi.org/10.1002/2015GL064048
1052 Stríkis, N.M., Cruz, F.W., Barreto, E.A.S., Naughton, F., Vuille, M., Cheng, H.,
1053 Voelker, A.H.L., Zhang, H., Karmann, I., Lawrence Edwards, R., Auler,
1054 A.S., Santos, R.V., Sales, H.R., 2018. South American monsoon response
1055 to iceberg discharge in the North Atlantic. Proc. Natl. Acad. Sci. U. S. A.
1056 115, 3788–3793. https://doi.org/10.1073/pnas.1717784115
1057 Sun, N., Brandon, A.D., Forman, S.L., Waters, M.R., Befus, K.S., 2020.
1058 Volcanic origin for younger dryas geochemical anomalies ca. 12,900 cal
1059 B.P. Sci. Adv. 6, 1–10. https://doi.org/10.1126/sciadv.aax8587
1060 Velay-Vitow, J., Richard Peltier, W., 2020. Out of the Ice Age: Megatides of the
1061 Arctic Ocean and the Bølling-Ållerød, Younger Dryas Transition. Geophys.
1062 Res. Lett. 47, 1–10. https://doi.org/10.1029/2020GL089870
1063 Venancio, I.M., Shimizu, M.H., Santos, T.P., Lessa, D.O., Portilho-Ramos, R.C.,
1064 Chiessi, C.M., Crivellari, S., Mulitza, S., Kuhnert, H., Tiedemann, R.,
1065 Vahlenkamp, M., Bickert, T., Sampaio, G., Albuquerque, A.L.S., Veiga, S.,
1066 Nobre, P., Nobre, C., 2020. Changes in surface hydrography at the western
1067 tropical Atlantic during the Younger Dryas. Glob. Planet. Change 184,
1068 103047. https://doi.org/10.1016/j.gloplacha.2019.103047

1069 Voelker, A.H.L., Abreu, L. de, 2013. A Review of Abrupt Climate Change Events
1070 in the Northeastern Atlantic Ocean (Iberian Margin): Latitudinal,
1071 Longitudinal, and Vertical Gradients. Abrupt Clim. Chang. Mech. Patterns,
1072 Impacts 15–37. https://doi.org/10.1029/2010GM001021
1073 Yarincik, K.M., Murray, R.W., Lyons, T.W., Peterson, L.C., Haug, G.H., 2000.
1074 Oxygenation history of bottom waters in the Cariaco Basin, Venezuela,
1075 over the past 578,000 years: Results from redox-sensitive metals (Mo, V,
1076 Mn, and Fe). Paleoceanography 15, 593–604.
1077 https://doi.org/10.1029/1999PA000401
1078 Zhang, Y., Chiessi, C.M., Mulitza, S., Sawakuchi, A.O., Häggi, C., Zabel, M.,
1079 Portilho-Ramos, R.C., Schefuß, E., Crivellari, S., Wefer, G., 2017. Different
1080 precipitation patterns across tropical South America during Heinrich and
1081 Dansgaard-Oeschger stadials. Quat. Sci. Rev. 177, 1–9.
1082 https://doi.org/10.1016/j.quascirev.2017.10.012

1083

1084 **FIGURE CAPTIONS**

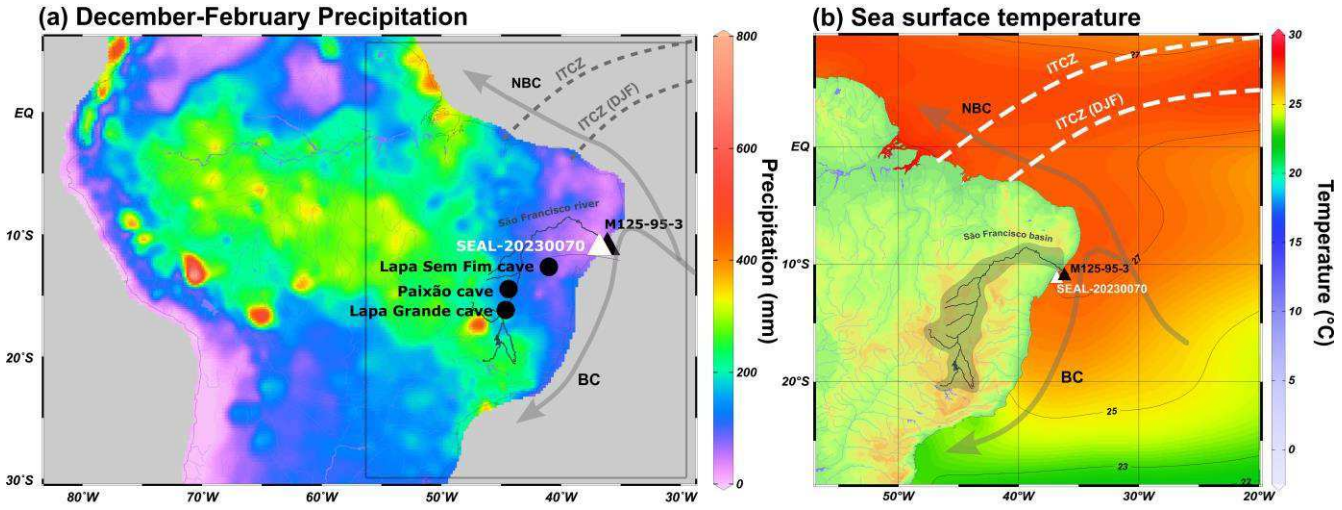

1085

1086 **Figure 1:** Location of marine sediment cores SEAL-202300070 (white triangle)
1087 and M125-95-3 (black triangle) investigated in this study. **(a)** Southern

Hemisphere summer (December-February - DJF) accumulated precipitation over tropical South America from the University of Delaware (http://climate.geog.udel.edu/~climate/). **(b)** Annual mean sea surface temperature (SST) in the western tropical Atlantic Ocean (Locarnini et al., 2013). Surface ocean currents are after Stramma and England (1999): North Brazil Current (NBC) and Brazil Current (BC). Thick dotted lines mark the approximate location of the Intertropical Convergent Zone (ITCZ) over the Atlantic Ocean. Maps generated with the software Ocean Data View (Schlitzer et al., 2016).

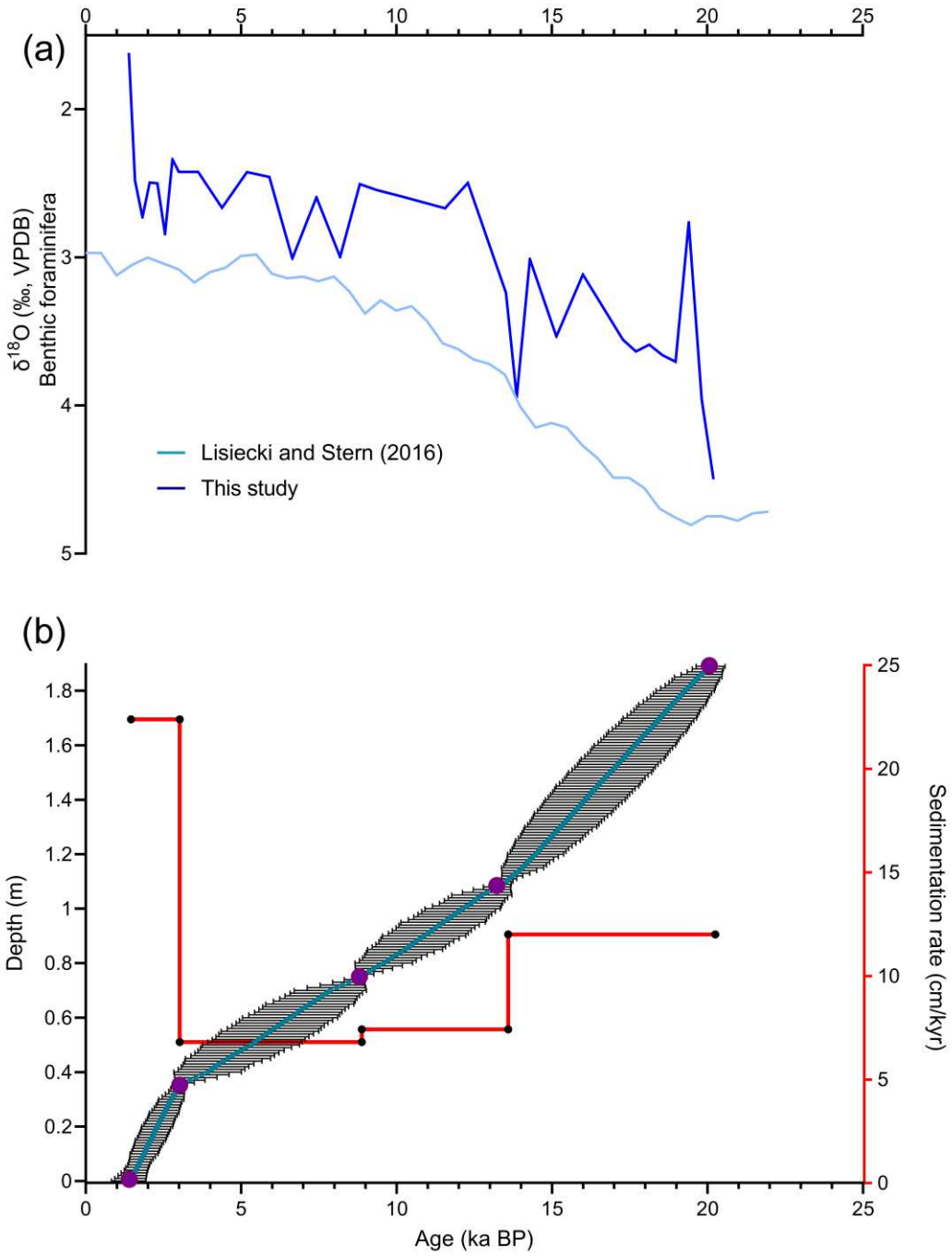

Figure 2: (a) Comparison between the benthic foraminiferal stable oxygen isotope ($\delta^{18}O$) record of core SEAL-202300070 and the benthic foraminiferal stack of Lisiecki and Stern, (2016) for intermediate waters in the South Atlantic. **(b)** Age model (based of five planktonic foraminiferal accelerator mass spectrometry ages and sedimentation rates (red curve) for core SEAL-

202300070, produced with the PaleoDataView version 0.9.5.5 software (Langner and Mulitza, 2019) and using the BACON v. 2.2 age modeling tool (Blaauw and Christen, 2011). For the age model, purple circles represent calibrated median radiocarbon ages, the central blue curve represents average ages, and error bars represent maximum and minimum ages.

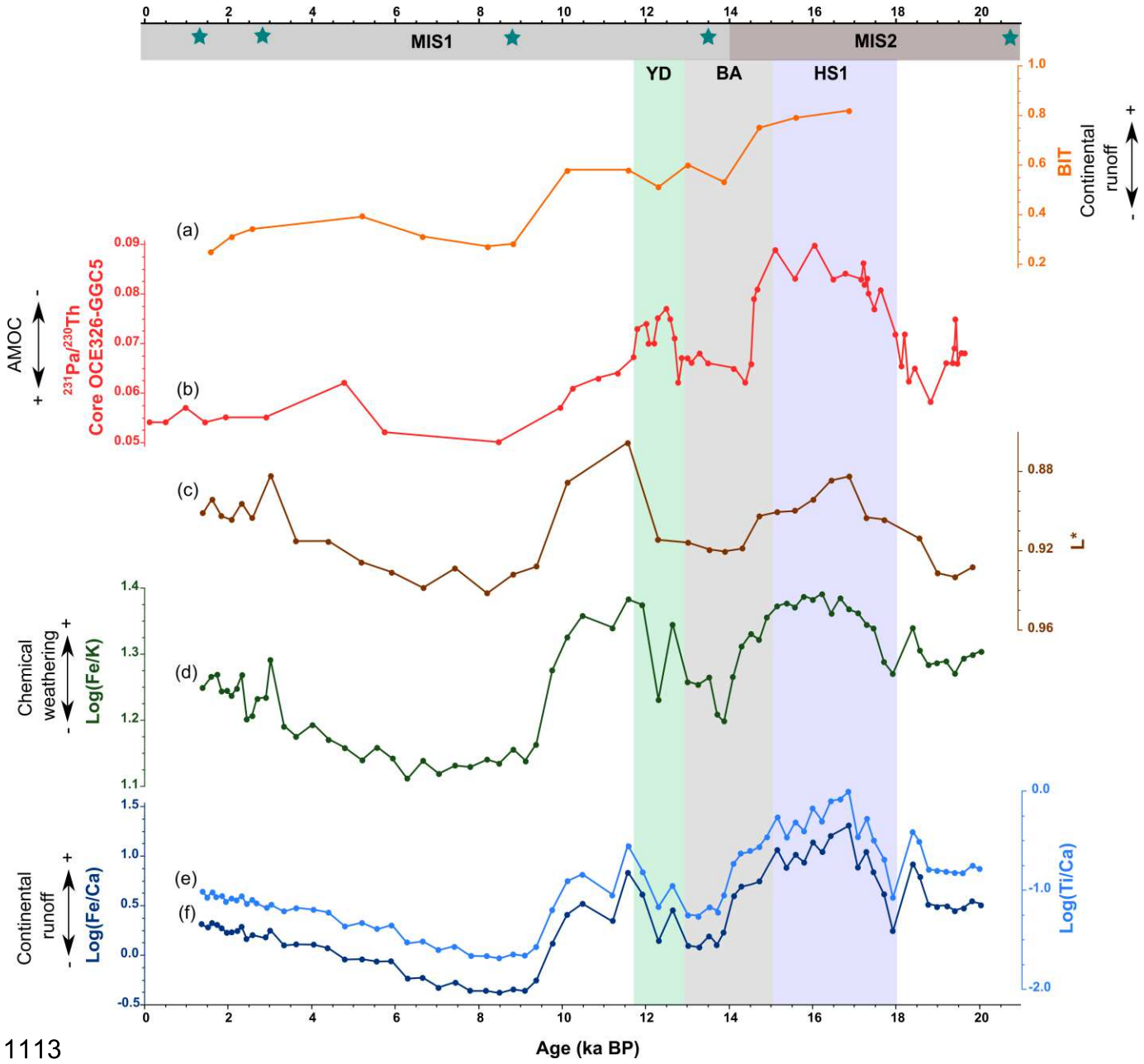

Figure 3: Geochemical records from core SEAL-202300070 for the last 20 kyr BP. **(a)** Branched and isoprenoid tetraether (BIT) index representing terrestrial vs marine contribution of organic matter, constructed using the ratio between Branched glycerol dialkyl glycerol tetraethers and crenarchaeol organic molecules. **(b)** Sedimentary $^{231}Pa/^{230}Th$ record from core GGC5 from the Bermuda Rise (McManus et al., 2004) for comparison. **(c)** Spectral reflectance (brightness) of the sediments in the visible spectrum (L*). X-rays fluorescence

(XRF)-derived log(Fe/K) **(d)**, log(Ti/Ca) **(e)** and log(Ti/Ca) **(f)**. Vertical bars mark the abrupt millennial scale events Heinrich Stadial 1 (HS1; blue shading), Bølling–Allerød (BA; lighter green shading) and Younger Dryas (YD; darker green shading). Marine isotope stages (MIS) are represented below the upper age axis. Green stars represent calibrated median radiocarbon ages.

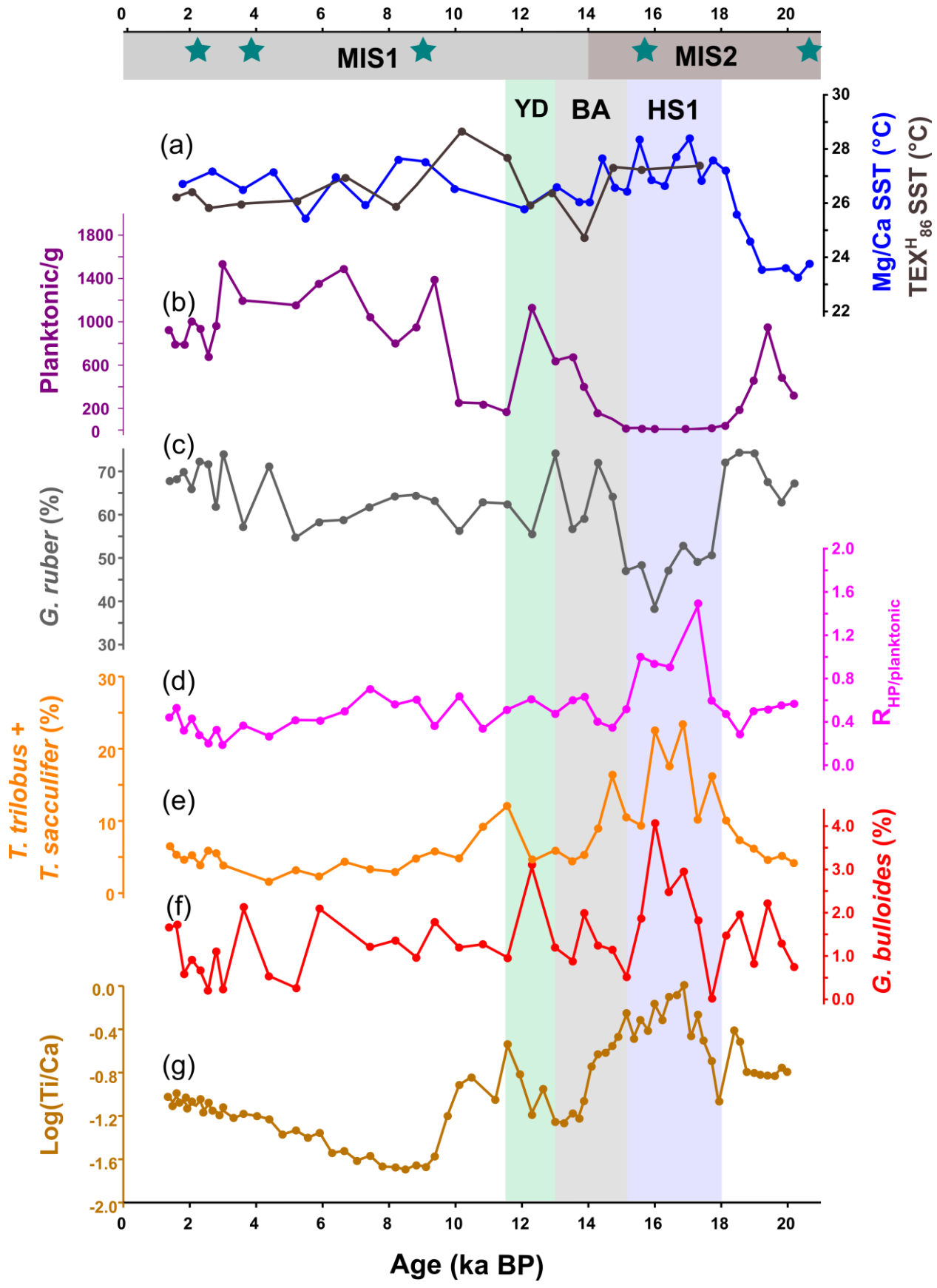
MIS1
MIS2
YD
BA
HS1
(a)
(b)
(c)
(d)
(e)
(f)
(g)
Mg/Ca SST (°C)
TEX$^{H}_{86}$ SST (°C)
Planktonic/g
G. ruber (%)
R$_{HP/planktonic}$
T. trilobus + T. sacculifer (%)
G. bulloides (%)
Log(Ti/Ca)
Age (ka BP)

Figure 4: Relative abundances of planktonic foraminiferal species at core SEAL-20230070 and reconstructed sea surface temperatures SSTs at cores SEAL-202300070 and M125-95-3 over the last 20 kyr. **(a)** Mg/Ca-based SST from core M125-93-3 (dark blue line; this study) and TEX^{H}_{86}-based SST from core SEAL-20230070. **(b)** Absolute planktonic foraminiferal abundances. **(c)** Relative abundance of *Globigerinoides ruber* **(d)** $R_{hp/planktonic}$ index. **(e)** Relative abundance of *Trilobatus trilobus* + *Trilobatus sacculifer;* **(f)** Relative abundance of *Globigerina bulloides* **(g)** X-rays fluorescence (XRF)-derived log(Ti/Ca). Horizontal bars mark the abrupt millennial scale events Heinrich Stadial 1 (HS1; blue shading), Bølling–Allerød (BA; lighter green shading) and Younger Dryas (YD; darker green shading). Marine isotope stages (MIS) are represented next to the upper age axis. Green stars represent calibrated radiocarbon ages.

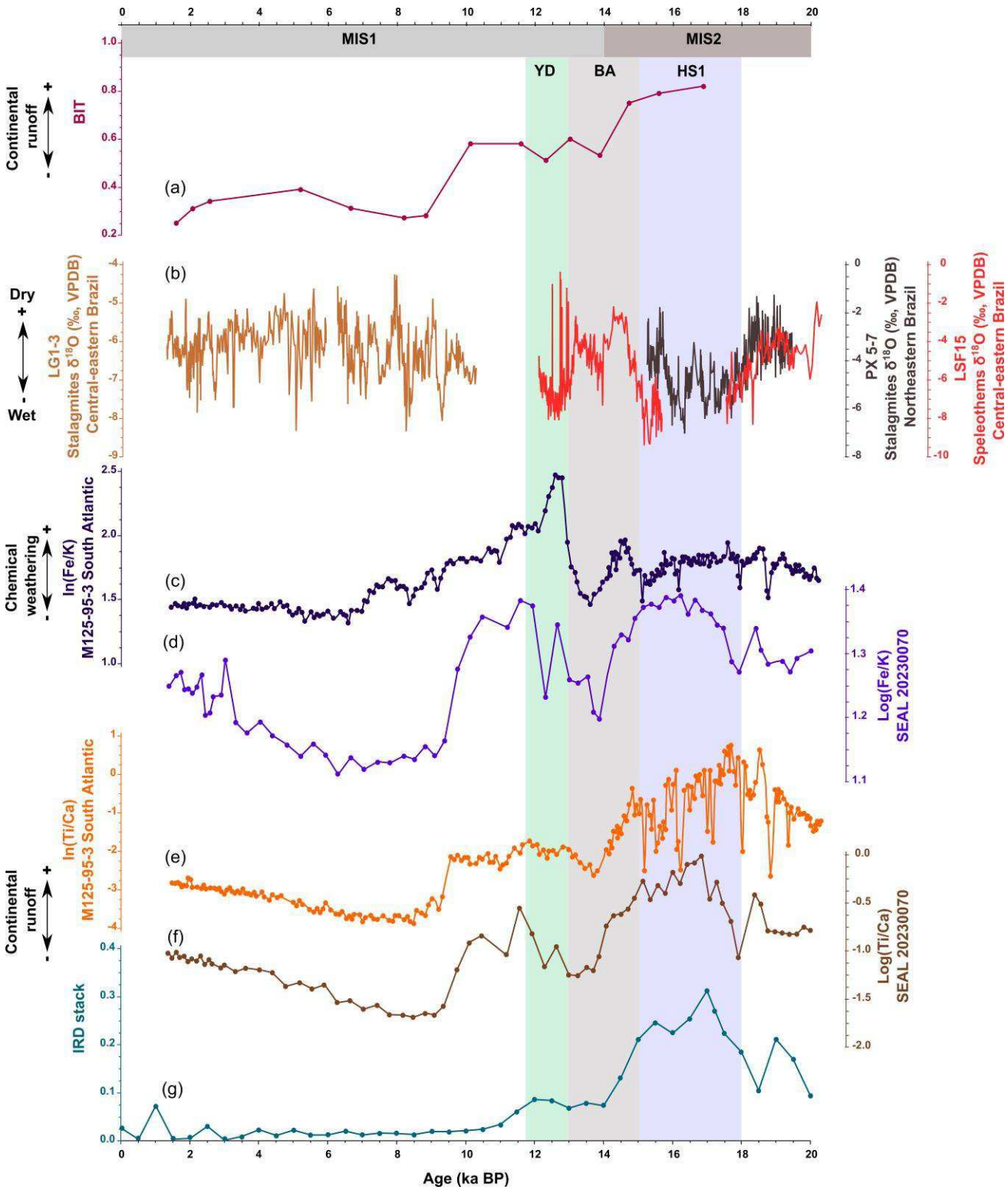

1139

1140 **Figure 5**: Paleoclimate records from the western tropical Atlantic and

1141 continental South America compared with a mid-latitude North Atlantic ice-

1142 rafted debris record. **(a)** Branched and isoprenoid tetraether (BIT) from marine

1143 sediment core SEAL-202300070 (this study). **(b)** Continental speleothem $\delta^{18}O$

records of the composite PX5 and PX7 speleothems from Paixão Cave (northeastern Brazil; black curve, Stríkis et al., 2015); LSF15 $\delta^{18}O$ speleothem record from the Lapa Sem Fim Cave (central-eastern Brazil; red curve, Stríkis et al., 2015); LG1-3 $\delta_{18}O$ speleothem record from the Lapa Grande Cave (central-eastern Brazil; orange curve, Stríkis et al., 2015). **(c)** X-ray fluorescence (XRF) scanner-derived ln(Fe/K) from core M125-95-3 (Campos et al., 2019). **(d)** Conventional XRF-derived log(Fe/K) at core SEAL-202300070 (this study). **(e)** XRF scanner-derived ln(Ti/Ca) from core M125-95-3 (Campos et al., 2019). **(f)** Conventional XRF-derived log(Ti/Ca) from core SEAL-202300070 (this study). **(g)** Ice rafted debris (IRD) record from the Iberian Margin (core MD95-2040) (Voelker and Abreu, 2013). Vertical bars mark the abrupt millennial scale events Heinrich Stadial 1 (HS1; blue shading), Bølling–Allerød (BA; lighter green shading) and the Younger Dryas (YD; darker green shading). Marine isotope (MIS) stages are represented below the upper age axis.

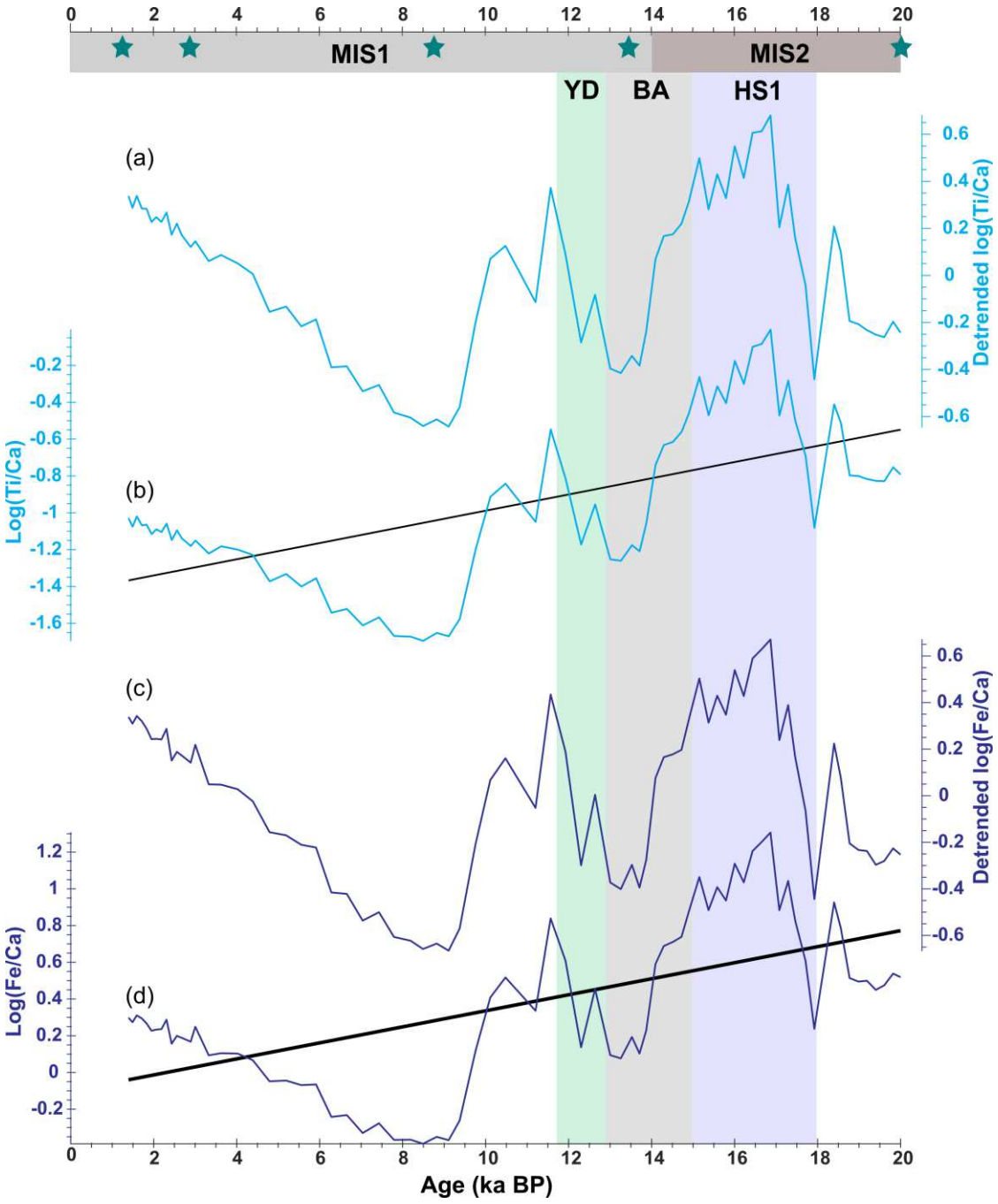

Figure 6: Detrended log(Ti/Ca) and log(Fe/Ca) at core SEAL-20230070. **(a)** X-rays fluorescence (XRF)-derived linearly detrended log(Ti/Ca) from core SEAL-202300070. **(b)** XRF-derived log(Ti/Ca) from core SEAL-202300070. **(c)** XRF-derived linearly detrended log(Fe/Ca) from core SEAL-202300070. **(d)** XRF-derived log(Fe/Ca) from core SEAL-202300070. Vertical bars mark the abrupt millennial scale events Heinrich Stadial 1 (HS1; blue shading), Bølling–Allerød

(BA; lighter green shading) and the Younger Dryas (YD; darker green shading). Marine isotope (MIS) stages are represented below the upper age axis. Green stars represent calibrated radiocarbon ages. Detrending was performed with the software Acycle version 2.0 (Li et al., 2019)

ANEXO A – COMPROVANTE DE SUBMISSÃO

De: em.palaeo.0.76c964.ef46755a@editorialmanager.com <em.palaeo.0.76c964.ef46755a@editorialmanager.com> em nome de Palaeogeography, Palaeoclimatology, Palaeoecology <em@editorialmanager.com>
Enviado: quarta-feira, 20 de outubro de 2021 13:14
Para: Alisson Klayton Martins <alissonkm@edu.unisinos.br>
Assunto: Confirming submission to Palaeogeography, Palaeoclimatology, Palaeoecology

This is an automated message.

Links between precipitation patterns over eastern tropical South America and primary productivity in the western tropical South Atlantic Ocean during the last 20 kyr

Dear Mr. Klayton Martins,

We have received the above referenced manuscript you submitted to Palaeogeography, Palaeoclimatology, Palaeoecology.

To track the status of your manuscript, please log in as an author at https://www.editorialmanager.com/palaeo/, and navigate to the "Submissions Being Processed" folder.

Thank you for submitting your work to this journal.

Kind regards,
Palaeogeography, Palaeoclimatology, Palaeoecology

More information and support

You will find information relevant for you as an author on Elsevier's Author Hub: https://www.elsevier.com/authors

FAQ: How can I reset a forgotten password?
https://service.elsevier.com/app/answers/detail/a_id/28452/supporthub/publishing/
For further assistance, please visit our customer service site: https://service.elsevier.com/app/home/supporthub/publishing/
Here you can search for solutions on a range of topics, find answers to frequently asked questions, and learn more about Editorial Manager via interactive tutorials. You can also talk 24/7 to our customer support team by phone and 24/7 by live chat and email

#AU_PALAEO#

To ensure this email reaches the intended recipient, please do not delete the above code

---

In compliance with data protection regulations, you may request that we remove your personal registration details at any time. (Use the following URL: https://www.editorialmanager.com/palaeo/login.asp?a=r). Please contact the publication office if you have any questions.